The International Journal of Advanced Manufacturing Technology (2022) 121:5731–5754
https://doi.org/10.1007/s00170-022-09463-y

ORIGINAL ARTICLE

Asymmetrical Pythagorean-hodograph spline-based C^4 continuous local corner smoothing method with jerk-continuous feedrate scheduling along linear toolpath

Xin Jiang[1,3,6] · Yifei Hu[1,2] · Guanying Huo[1,3,6] · Cheng Su[1,3,5] · Bolun Wang[7] · Hexiong Li[1,2] · Li-Yong Shen[4] · Zhiming Zheng[1,3,6]

Received: 23 September 2021 / Accepted: 31 May 2022 / Published online: 30 July 2022

Abstract

In computer numerical control systems, linear segments generated by computer-aided manufacturing software are the most widely used toolpath format. Since the linear toolpath is discontinuous at the junction of two adjacent segments, the fluctuations on velocity, acceleration and jerk are inevitable. Local corner smoothing is widely used to address this problem. However, most existing methods use symmetrical splines to smooth the corners. When any one of the linear segments at the corner is short, the inserted spline will be micro to avoid overlap. This will increase the curvature extreme of the spline and reduce the feedrate on it. In this article, the corners are smoothed by a C^4 continuous asymmetric Pythagorean-hodograph (PH) spline. The curvature extreme of the proposed spline is investigated first, and $K = 2.5$ is determined as the threshold to constrain the asymmetry of the spline. Then, a two-step strategy is used to generate a blended toolpath composed of asymmetric PH splines and linear segments. In the first step, the PH splines at the corners are generated under the condition that the transition lengths do not exceed half of the length of the linear segments. In the second step, the splines at the corners are re-planned to reduce the curvature extremes, if the transition error does not reach the given threshold and there are extra linear trajectories on both sides of the spline trajectory. Finally, the bilinear interpolation method is applied to determine the critical points of the smoothed toolpath, and a jerk-continuous feedrate scheduling scheme is presented to interpolate the smoothed toolpath. Simulations show that, under the condition of not affecting the machining quality, the proposed method can improve the machining efficiency by 7.27 to 75.11% compared to G^3 and G^4 methods.

Keywords Local corner smoothing · Pythagorean-hodograph spline · Continuity · Jerk-continuous feedrate scheduling

1 Introduction

To machine 3D products with freeform surfaces, computer-aided design (CAD) models are designed first, Then, the cutter contact (CC) paths are converted into the cutter location (CL) paths by the computer-aided manufacturing (CAM) software. Since the linear interpolation (G01) is supported by all multi-axis computer numerical control (CNC) machining, the CL paths are usually divided into a large number of linear trajectories as the toolpath to guide the movement of machine axes [1]. However, due to the tangential discontinuities at the intersection of linear paths, there will be infinite acceleration of axes and discontinuous motion, which will excite structural vibration. If it is simply planned to stop at the corner junction, frequent acceleration and deceleration processes are inevitable, which will increase machining time significantly [2]. Therefore, to improve machining efficiency and

✉ Guanying Huo
gyhuo@buaa.edu.cn

✉ Cheng Su
sucheng1991@buaa.edu.cn

[1] Key Laboratory of Mathematics, Informatics and Behavioral Semantics (LMIB), Institute of Artificial Intelligence, Beihang University, Beijing, China

[2] School of Mathematics Science, Shenyuan Honors College, Beihang University, Beijing, China

[3] Zhengzhou Aerotropolis Institute of Artificial Intelligence, Henan, Zhengzhou, China

[4] School of Mathematical Sciences, University of Chinese Academy of Sciences, Beijing, China

[5] School of Computer Science and Engineering, Beihang University, Beijing, China

[6] Peng Cheng Laboratory, Guangdong, Shenzhen, China

[7] Visual Computing Center, King Abdullah University of Science and Technology, Thuwal, Saudi Arabia

quality, the toolpath should be processed to get higher order continuity [3]. The approaches can be divided into global smoothing [4–8] and local smoothing [3, 9–29] methods.

The global smoothing methods usually utilize one or several smooth spline curves, such as B-splines, polynomial splines and non-uniform rational B-spline (NURBS) curves to approximate the discrete G01 points. The high-order continuity of the proposed curves makes them guarantee smoothness along the entire toolpath [9]. However, they have shortages such as numerical instability, lack of chord error constraint and lack of assurance result [4].

The local smoothing methods usually replace the shape corners with one or a pair of micro-curves [10], among which the spline trajectory, such as B-spline and Bezier, has attracted more interests of the researchers.

B-spline and Bezier spline are the most widely used transition curves to achieve second-order geometric (G^2) continuity or second-order parametric (C^2) continuity. Zhao et al. [11] adopted a cubic B-spline with five control points to smooth the adjacent linear segments, which made the overall smoothed path C^2 continuous. Sencer and Shamoto [12] employed a quintic Bezier curve to blend the adjacent straight lines, and the curvature extreme was minimized for higher machining efficiency. In [13], a two-step strategy was proposed to generate G^2 continuous toolpath, where the curvature energy of the cubic Bezier curve was minimized first, then the optimal transition length was determined by minimizing the sum of two curvature extremes. Jin et al. [14] proposed a transition method for five-axes machining in workpiece coordinate system (WCS), which utilized a dual-Bezier splines as transition curves. Bi et al. [15] developed a G^2 continuous transition method with a cubic Bezier curve; the approximation error at the segment junction can be accurately guaranteed, and the curvature extreme can be analytically computed and optimized. These methods [11–15] above can only guarantee that the toolpath is C^2 or G^2 continuous; however, higher continuity is desired to obtain smooth feedrate profile. Tulsyan and Altintas [16] inserted a quintic B-spline with seven control points for tool tip at the adjacent linear segments and a septic B-spline with nine unit control vectors for the tool orientation. The optimal control points and vectors were calculated to generate C^3 continuous toolpath. In [17], two symmetric quartic Bezier curves were proposed to generate C^3 interpolative toolpath, and a jerk-continuous feedrate scheduling was given. Zhang et al. [18] proposed a symmetric quartic B-spline curve to smooth the tool tip position in WCS and an asymmetric quartic B-spline curve to smooth the tool orientation in machine coordinate system (MCS), which constrained both errors of tool tip position and tool orientation in WCS. In addition, Xie et al. [19] employed a single quintic B-spline with seven control points to achieve G^3 continuity and applied it to five degrees of freedom (5-DoF) machining robot. In [3], by adopting a quintic B-spline with nine control points, the toolpath was improved to G^4 continuous, and a corresponding jerk-smooth feedrate scheduling scheme was presented.

Although B-spline and Bezier spline can smooth the toolpath, their arc lengths have no analytical solutions respect with spline parameters, which makes it difficult to calculate the next parameter in the fine interpolation. To overcome this problem, the clothoid spline-based methods [10, 20–24] and Pythagorean-hodograph (PH) spline-based methods [9, 25–29] have been developed. Shahzadeh et al. [22] used biclothoid fillets as transition curves to smooth the corners and ensure the G^2 continuity of the toolpath. The main advantage of this fillet fitting method was that it was not limited to line to line transitions; it can smooth two arcs or a line and arc as well. In [23], the traditional clothoid was extended from 2 to 3 dimensions, which can achieve a higher degree of continuity, i.e. G^3 continuity. Huang et al. [24] proposed a novel curve 'airthoid' based on clothoid spline, then the biairthoid was involved to smooth the corners of the tool position in the WCS and the corners of the tool orientation in the MCS. In [10], a novel smoothing method based on a pair of clothoid splines was proposed to realize the integral planning of the geometrical curve and the feedrate profile, which can achieve the adaptive contour accuracy. Since the clothoid is defined with respect to the Fresnel integral, which cannot be calculated analytically, these methods can only be carried out offline. In [26], the sharp corners on the toolpath were interpolated with PH interpolation, which minimized the geometric and interpolator approximation errors simultaneously. Shi et al. [29] proposed a smoothing method by using a pair of quintic PH curves to round the corners of linear five-axis tool path. Hu et al. [9] applied a quintic PH spline with twelve control points to achieve C^3 continuity. In [30], an asymmetrical PH spline-based C^3 continuous corner smoothing algorithm was developed for five-axis tool paths with short segments. However, they were limited to the second-order or third-order continuity. When the fourth-order continuity is reached, the first and second curvature derivatives are both continuous along the combined toolpath; the jerk and jounce are both continuous if a smooth jerk profile is proposed in feedrate scheduling, which can reduce vibration and tracking error [3].

In this paper, the asymmetric PH spline with sixteen control points is developed and inserted among linear toolpath segments. The control points are optimized to decrease the curvature extreme of the proposed PH spline and achieve C^4 continuity of the combined toolpath. A corresponding jerk-continuous feedrate scheduling scheme is also presented to interpolate the toolpath. The remainder of this paper is organized as follows. In Sect. 2, the basic concepts of the proposed PH spline are introduced, and the curvature extreme is investigated. Section 3 provides a PH spline curve transition method to generate C^4 smooth path. In Sect. 4, a jerk-continuous feedrate scheduling scheme is given. Section 5 presents the simulations, and the results are compared with two conventional methods. Finally, Sect. 6 gives the conclusions and future works.

2 Introduction of the proposed transition curve

2.1 Introduction of planar Pythagorean-hodograph spline

A planar parameter curve $r(t) = (x(t), y(t))$ is called Pythagorean-hodograph (PH) curve, if it satisfies

$$x^2(t) + y^2(t) = \sigma^2(t) \tag{1}$$

where $\sigma(t)$ is the parametric speed of $r(t)$ and also a polynomial respect with t. To get a PH curve, usually let $x'(t) = u^2(t) - v^2(t)$ and $y'(t) = 2u(t)v(t)$, where $u(t)$ and $v(t)$ are two relatively prime polynomials, so $\sigma(t) = |r'(t)| = \sqrt{x'^2(t) + y'(t)} = u^2(t) + v^2(t)$, which is a polynomial.

Let $u(t) = \sum_{i=0}^{m} u_i b_i^m(t)$ and $v(t) = \sum_{i=0}^{m} v_i b_i^m(t)$, where $u_i = [ux_i, uy_i]^T$ and $v_i = [vx_i, vy_i]^T$ are control points, m is the degree of these two spline function. $b_i^m(t) = \binom{m}{i} t^i (1-t)^{m-i}$ are the Bezier basis functions, where $\binom{m}{i} = \frac{m!}{i!(m-i)!}$. Integrating $x'(t)$ and $y'(t)$ gives the planar PH spline $r(t) = \sum_{i=0}^{n} B_i b_i^n(t)$, where $n = 2m + 1$. $B_i = [x_i, y_i]^T$ are control points, which will be detailed in the next section. The parametric speed function can be written as $\sigma(t) = \sum_{i=0}^{n-1} \sigma_i b_i^{n-1}(t)$; $\sigma_i = [\sigma x_i, \sigma y_i]^T$ are control points, which can be calculated by the following formula:

$$\sigma_i = \sum_{j=max(0,i-m)}^{min(m,i)} \frac{\binom{m}{j}\binom{m}{i-j}}{\binom{n-1}{i}} (u_j u_{i-j} + v_j v_{i-j}), \quad i = 0, 1, \ldots, n-1 \tag{2}$$

The cumulative arc length function $s(t)$ of $r(t)$ can be obtained by integrating $\sigma(t)$; we arrive at

$$\begin{cases} s(t) = \sum_{i=0}^{n} s_i b_i^m(t) \\ s_0 = 0, s_i = \frac{1}{n}\sum_{j}^{i-1} \sigma_j, i = 1, 2, \ldots, n \end{cases} \tag{3}$$

As can be seen from Eq. (3), $s(t)$ is also a polynomial respect with t, which makes PH spline of great application value in interpolation.

2.2 Design of the PH transition curve

In this research, a C^4 continuous PH spline is inserted to smoothly transition two successive linear segments. It has been proved that only when $m \geq 7$ can a C^4 continuous PH spline be designed [27]. For simplicity, let $m = 7$; then, $u(t) = \sum_{i=0}^{7} u_i b_i^7(t)$ and $v(t) = \sum_{i=0}^{7} v_i b_i^7(t)$. The designed C^4 continuous PH spline is written as

$$r(t) = (x(t), y(t)) = \sum_{i=0}^{15} B_i b_i^{15}(t), t \in [0, 1] \tag{4}$$

where $B_i (i = 0, 1, 2, \ldots, 15)$ are control points, which will be given later.

As shown in Fig. 1, the corner is formed by two linear segments, i.e. P_0P_1 and P_1P_2; their unit directions are $T_1 = \overrightarrow{P_0P_1} / \left|\overrightarrow{P_0P_1}\right|$ and $T_2 = \overrightarrow{P_1P_2} / \left|\overrightarrow{P_1P_2}\right|$. θ is the angle between these two unit directions, which can be calculated by

$$\theta = arccos(T_1 \cdot T_2) \tag{5}$$

$\{B_0, B_1, \ldots, B_{15}\}$ are the sixteen control points of the proposed PH curve. From Ref. [9], the transition curve is C^4 continuous only when the first five control points $\{B_0, B_1, B_2, B_3, B_4\}$ lie in segment P_0P_1, the last five control points $\{B_{11}, B_{12}, B_{13}, B_{14}, B_{15}\}$ lie in segment P_1P_2 and they meet the following equations:

$$\overrightarrow{B_0B_1} = \overrightarrow{B_1B_2} = \overrightarrow{B_2B_3} = \overrightarrow{B_3B_4} \tag{6}$$

$$\overrightarrow{B_{11}B_{12}} = \overrightarrow{B_{12}B_{13}} = \overrightarrow{B_{13}B_{14}} = \overrightarrow{B_{14}B_{15}}. \tag{7}$$

To make the control points meet the above conditions, $\{u_0, u_1, u_2, u_3, u_4, u_5, u_6, u_7\}$ and $\{v_0, v_1, v_2, v_3, v_4, v_5, v_6, v_7\}$ should satisfy the following relationship:

$$\begin{cases} u_0 = u_1 = u_2 = u_3 \\ u_4 = u_5 = u_6 = u_7 \\ v_0 = v_1 = v_2 = v_3 \\ v_4 = v_5 = v_6 = v_7 \end{cases} \tag{8}$$

Then, the control points$B_i (i = 0, 1, 2, \ldots, 15)$, $u_i (i = 0, 1, 2, \ldots, 7)$ and $v_i (i = 0, 1, 2, \ldots, 7)$ have the following relation:

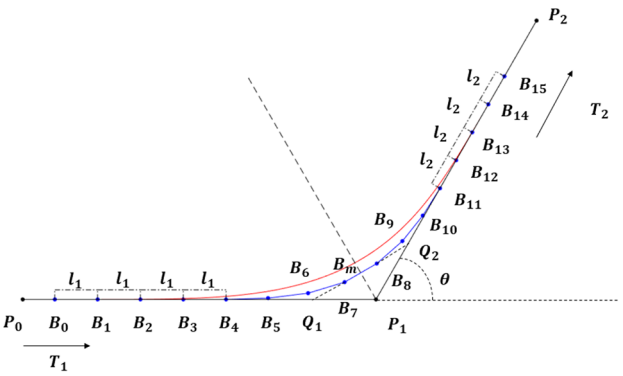

Fig. 1 Description of the C^4 transition curve

$$\begin{cases} \overrightarrow{B_0B_1}=\overrightarrow{B_1B_2}=\overrightarrow{B_2B_3}=\overrightarrow{B_3B_4}=\overrightarrow{n_1} \\ \overrightarrow{B_4B_5}=\frac{133}{143}\overrightarrow{n_1}+\frac{10}{143}\overrightarrow{m} \\ \overrightarrow{B_5B_6}=\frac{105}{143}\overrightarrow{n_1}+\frac{38}{143}\overrightarrow{m} \\ \overrightarrow{B_6B_7}=\frac{175}{429}\overrightarrow{n_1}+\frac{254}{429}\overrightarrow{m} \\ \overrightarrow{B_7B_8}=\overrightarrow{m} \\ \overrightarrow{B_8B_9}=\frac{175}{429}\overrightarrow{n_2}+\frac{254}{429}\overrightarrow{m} \\ \overrightarrow{B_9B_{10}}=\frac{105}{143}\overrightarrow{n_2}+\frac{38}{143}\overrightarrow{m} \\ \overrightarrow{B_{10}B_{11}}=\frac{133}{143}\overrightarrow{n_2}+\frac{10}{143}\overrightarrow{m} \\ \overrightarrow{B_{11}B_{12}}=\overrightarrow{B_{12}B_{13}}=\overrightarrow{B_{13}B_{14}}=\overrightarrow{B_{14}B_{15}}=\overrightarrow{n_2} \end{cases} \tag{9}$$

where $\overrightarrow{n_1}=\left(u_0^2-v_0^2,2u_0v_0\right)^T/15$, $\overrightarrow{n_2}=\left(u_7^2-v_7^2,2u_7v_7\right)^T/15$ and $\overrightarrow{m}=\left(u_0u_7-v_0v_7,u_0v_7+u_7v_0\right)^T/15$.

To get the relationship between the control points and the corner point P_1, two theorems are given as follows:

Theorem 1 *Let* $\overrightarrow{n_1}=l_1\overrightarrow{T_1}$ *and* $\overrightarrow{n_2}=l_2\overrightarrow{T_2}$, *then* $\left|\overrightarrow{B_7B_8}\right|=|\overrightarrow{m}|=\sqrt{l_1l_2}$. *In addition,* $\frac{\overrightarrow{B_7B_8}}{\left|\overrightarrow{B_7B_8}\right|}=\frac{\overrightarrow{T_1}+\overrightarrow{T_2}}{\left|\overrightarrow{T_1}+\overrightarrow{T_2}\right|}$ *if the values of* u_0, v_0, u_7 *and* v_7 *are determined appropriately.*

Theorem 2 *Extend linear segment* B_7B_8 *from both ends to intersect* P_0P_1 *and* P_1P_2 *at* Q_1 *and* Q_2 *respectively, then* $\left|\overrightarrow{B_4Q_1}\right|=\frac{889}{429}l_1$, $\left|\overrightarrow{B_{11}Q_2}\right|=\frac{889}{429}l_2$ *and* $\left|\overrightarrow{Q_1P_1}\right|=\left|\overrightarrow{Q_2P_1}\right|=\frac{1225\sqrt{l_1l_2}}{858\cos\frac{\theta}{2}}$.

The proof process of Theorems 1 and 2 can be found in Appendices 1 and 2 respectively. According to these two theorems, the relation between the control points and the corner point P_1 is as follows:

$$\begin{cases} B_0=P_1-\left(4l_1+\frac{889}{429}l_1+l\right)\overrightarrow{T_1} \\ B_1=B_0+l_1\overrightarrow{T_1} \\ B_2=B_1+l_1\overrightarrow{T_1} \\ B_3=B_2+l_1\overrightarrow{T_1} \\ B_4=B_3+l_1\overrightarrow{T_1} \\ B_5=B_4+\frac{10}{143}\overrightarrow{m}+\frac{133}{143}l_1\overrightarrow{T_1} \\ B_6=B_5+\frac{38}{143}\overrightarrow{m}+\frac{105}{143}l_1\overrightarrow{T_1} \\ B_7=B_6+\frac{254}{429}\overrightarrow{m}+\frac{175}{429}l_1\overrightarrow{T_1} \\ B_8=B_7+\overrightarrow{m} \\ B_9=B_8+\frac{254}{429}\overrightarrow{m}+\frac{175}{429}l_2\overrightarrow{T_2} \\ B_{10}=B_9+\frac{38}{143}\overrightarrow{m}+\frac{105}{143}l_2\overrightarrow{T_2} \\ B_{11}=B_{10}+\frac{10}{143}\overrightarrow{m}+\frac{133}{143}l_2\overrightarrow{T_2} \\ B_{12}=B_{11}+l_2\overrightarrow{T_2} \\ B_{13}=B_{12}+l_2\overrightarrow{T_2} \\ B_{14}=B_{13}+l_2\overrightarrow{T_2} \\ B_{15}=B_{14}+l_2\overrightarrow{T_2} \end{cases} \tag{10}$$

where $\overrightarrow{m}=\sqrt{l_1l_2}\frac{\overrightarrow{T_1}+\overrightarrow{T_2}}{\left|\overrightarrow{T_1}+\overrightarrow{T_2}\right|}$, $l=\frac{1225\sqrt{l_1l_2}}{858cos\frac{\theta}{2}}$. It can be seen from Eq. (10) that for a certain corner, once l_1 and l_2 are determined, all control points are determined, which means the transition curve is determined.

To calculate the arc length of the proposed PH spline, the parametric speed function should be obtained first. Applying $m=7$, $n=15$ and Eq. (8) into Eq. (2), the control points of the parametric speed function $\sigma(t)=\sum_{i=0}^{14}\sigma_i b_i^{n-1}(t)$ are as follows:

$$\begin{cases} \sigma_0=\sigma_1=\sigma_2=\sigma_3=u_0^2+v_0^2 \\ \sigma_4=\frac{10}{143}\times(u_0u_7+v_0v_7)+\frac{133}{143}\times(u_0^2+v_0^2) \\ \sigma_5=\frac{38}{143}\times(u_0u_7+v_0v_7)+\frac{105}{143}\times(u_0^2+v_0^2) \\ \sigma_6=\frac{254}{429}\times(u_0u_7+v_0v_7)+\frac{175}{429}\times(u_0^2+v_0^2) \\ \sigma_7=u_0u_7+v_0v_7 \\ \sigma_8=\frac{254}{429}\times(u_0u_7+v_0v_7)+\frac{175}{429}\times(u_7^2+v_7^2) \\ \sigma_9=\frac{38}{143}\times(u_0u_7+v_0v_7)+\frac{105}{143}\times(u_7^2+v_7^2) \\ \sigma_{10}=\frac{10}{143}\times(u_0u_7+v_0v_7)+\frac{133}{143}\times(u_7^2+v_7^2) \\ \sigma_{11}=\sigma_{12}=\sigma_{13}=\sigma_{14}=u_7^2+v_7^2 \end{cases} \tag{11}$$

where $u_0^2+v_0^2=15l_1$ and $u_7^2+v_7^2=15l_2$; the only unknown value is $u_0u_7+v_0v_7$. From Eq. (9), $\overrightarrow{B_4B_5}=\frac{10}{143}\overrightarrow{n_1}+\frac{133}{143}\overrightarrow{m}=\frac{10}{143}\times\frac{1}{15}\left(u_0^2-v_0^2,2u_0v_0\right)^T+\frac{133}{143}\times\frac{1}{15}\left(u_0u_7-v_0v_7,u_0v_7+u_7v_0\right)^T$. Considering the length of vector $\overrightarrow{B_4B_5}$, then $(143\times15\times\left|\overrightarrow{B_4B_5}\right|)^2=10^2\times(u_0^2+v_0^2)\times(u_7^2+v_7^2)+133^2\times\left(u_0^2+v_0^2\right)^2+2\times10\times133\times(u_0u_7+v_0v_7)\times\left(u_0^2+v_0^2\right)$, $u_0u_7+v_0v_7$ can be calculated as

$$u_0u_7+v_0v_7=\frac{(2145\left|B_4B_5\right|)^2-22500l_1l_2-(1995l_1)^2}{39900l_1}. \tag{12}$$

As the parametric speed function is known, the cumulative arc length function $s(t)=\sum_{i=0}^{15}s_ib_i^{15}(t)$ can be obtained by substituting Eq. (11) into Eq. (3), which is omitted here.

2.3 The curvature extreme of the proposed PH spline

In feedrate scheduling, the feedrate is constrained by the curvature of the tool path, and the tool path is usually divided into several blocks according to critical points, where the points with local curvature extreme are usually regarded as critical points [31]. In this section, the curvature extreme of the proposed PH spline and the parameter of curvature extreme point are investigated.

From the previous section, the proposed PH spline is determined by two characteristic lengths l_1 and l_2, the corner point P_1 and two unit directions T_1 and T_2. Since the

Fig. 2 The curvature extreme of the proposed PH spline with various characteristic length l_2 and the corner angle. (**a**) $\theta = \pi/4$. (**b**) $\theta = \pi/2$. (**c**) $\theta = 3\pi/4$

curvature is intrinsic geometries, which is not affected by the selection of coordinate system, the curvature of the proposed PH spline is determined only by two characteristic lengths l_1, l_2 and the corner angle θ. Without loss of generality, let $l_2 \geq l_1$. In addition, when the ratio of l_2 and l_1 and corner angle θ are fixed, the curvature of each point at the proposed PH spline is inversely proportional to l_1; then, the value of l_1 does not affect the trend of curvature on the proposed PH spline. For simplicity, we let $l_1 = 1$mm; l_2 varies from 1 to 10mm in steps of 0.01mm, and θ varies from 0 to π in steps of $\frac{\pi}{180}$. To calculate the curvature extreme of the proposed PH spline, we take 0.001 as the parameter step to sample the points on the proposed PH spline and calculate its curvature; the largest one is recorded as the curvature extreme, and the corresponding parameter is recorded as the parameter of the curvature extreme point. When $\theta = \pi/4, \theta = \pi/2$ and $\theta = 3\pi/4$, the curvature extreme of the proposed PH spline with different characteristic length l_2 is calculated and shown as follows:

As can be seen from Fig. 2, even for different corner angles, the curvature extreme of the proposed PH spline has the same change trend: as the characteristic length l_2 is increased, the curvature extreme is first reduced and then increased. For a given corner angle θ, the characteristic length l_2 is limited by the length of the linear trajectory in the corner smoothing process. In most cases, l_2 cannot equal to the value (the abscissa of the red points in Fig. 2) that makes the curvature extreme of the proposed PH spline minimal. As an alternative, an optimal value for l_2 is determined by the following steps:

Step 1: Initialize $l_2 = 1$mm, Calculate the curvature extreme K_1.
Step 2: If $l_2 < 10$mm, $l_2 = l_2 + \Delta l$, where Δl is a small increment and $\Delta l = 0.01$mm is chosen in the searching algorithm, go to Step 3; otherwise, go to Step 5.
Step 3: Calculate the curvature extreme K_2. If $\frac{K_1 - K_2}{K_1} > \delta$, where δ is a small scalar and $\delta = 0.08\%$ is chosen in the searching algorithm, then $K_1 = K_2$, go to Step 2; otherwise, go to Step 4.
Step 4: The optimal value equals to $l_2 - \Delta l$; terminate the algorithm.
Step 5: The optimal value equals to l_2; terminate the algorithm.

Following the above algorithm, the optimal value for l_2 and corresponding curvature extreme for three different corner angles are obtained and shown as the blue points in

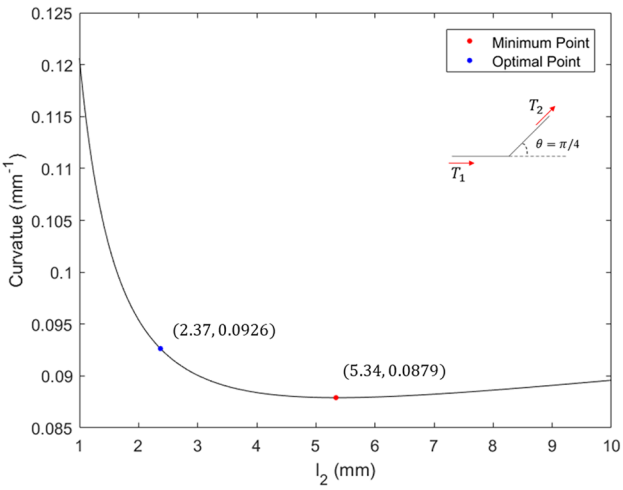

(a)

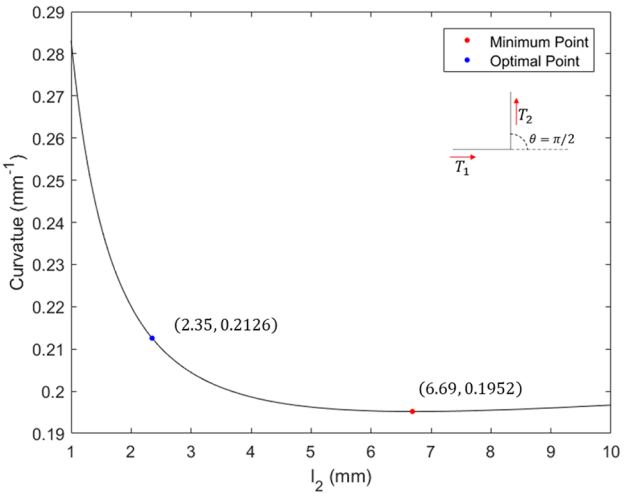

(b)

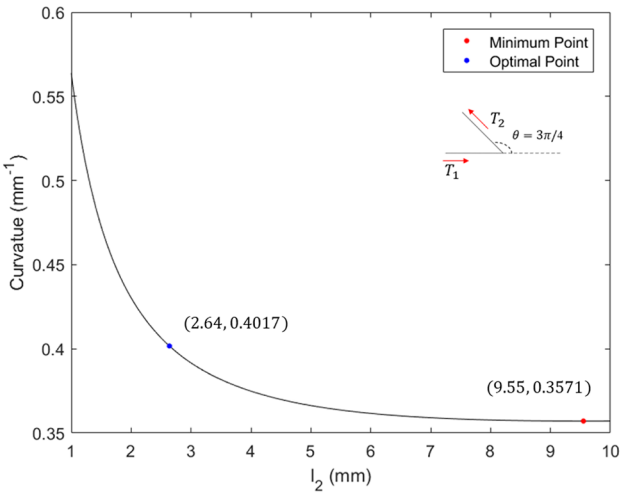

(c)

Fig. 2. Similarly, the curvature extreme of the proposed PH spline with different characteristic length l_2 and corner angle θ is calculated and shown in Fig. 3. The blue curve represents the optimal value for l_2 and its corresponding curvature extreme at different angles. The red curve represents the value for l_2 that makes the curvature extreme of the proposed PH spline minimal and its corresponding curvature extreme at different angles. It can be observed that at different angles, the optimal value for l_2 is between 2mm and 3mm. For simplicity, $K = 2.5$ is selected as the threshold of the ratio between l_1 and l_2, which will play an important role in the process of determining the characteristic lengths in the next section. Since the curvature extreme points will be regarded as critical points in feedrate scheduling, to detect the curvature extreme point of the inserted PH spline quickly, the parameters of the curvature extreme points on the proposed PH spline with various characteristic length l_2 and the corner angle θ are stored in matrix M, where $M(i,j)$ represents the parameter of the curvature extreme point when $l_1 = 1\text{mm}$, $l_2 = (0.99 + 0.01 \times j)\text{mm}$ and $\theta = (i-1) \times \pi/180$. The parameters of the curvature extreme points on the proposed PH spline with various characteristic length l_2 and the corner angle θ are shown as Fig. 4. Since $K = 2.5$ is selected as the threshold to constrain the ratio between l_1 and l_2, only the parts where l_2 is between 1mm and 3mm are displayed.

3 Generation of C^4 smooth path

3.1 Error constraint

As shown in Fig. 1, the proposed PH spline introduces a geometric deviation compared to the original toolpath, which should be constrained in the path-smoothing method for NC machining. Assuming the maximum geometric error allowed by the CNC systems is denoted as ε, then the two characteristic lengths l_1 and l_2 should be determined appropriately so that the actual geometric error is not greater than the given threshold. Before giving the constraint of l_1 and l_2, two theorems are given as follows:

Theorem 3 *If $l_1 = l_2$, then the maximum deviation is at the middle of the PH spline curve and calculated as.*

$$e_{max} = |r(0.5) - P_1| = \frac{1}{2^{14}} sin\left(\frac{\theta}{2}\right) \left[\left(\frac{397}{429} + 10207\right) l_1 + \frac{16384 \times 1225}{858 cos(\frac{\theta}{2})} l_1\right]. \tag{13}$$

Theorem 4 *Let $R(t)$ be the transition PH spline with equal characteristic lengths $l_0 = max(l_1, l_2)$, denote the maximal deviation between the linear trajectory P_0–$P_1 - P_2$ and the*

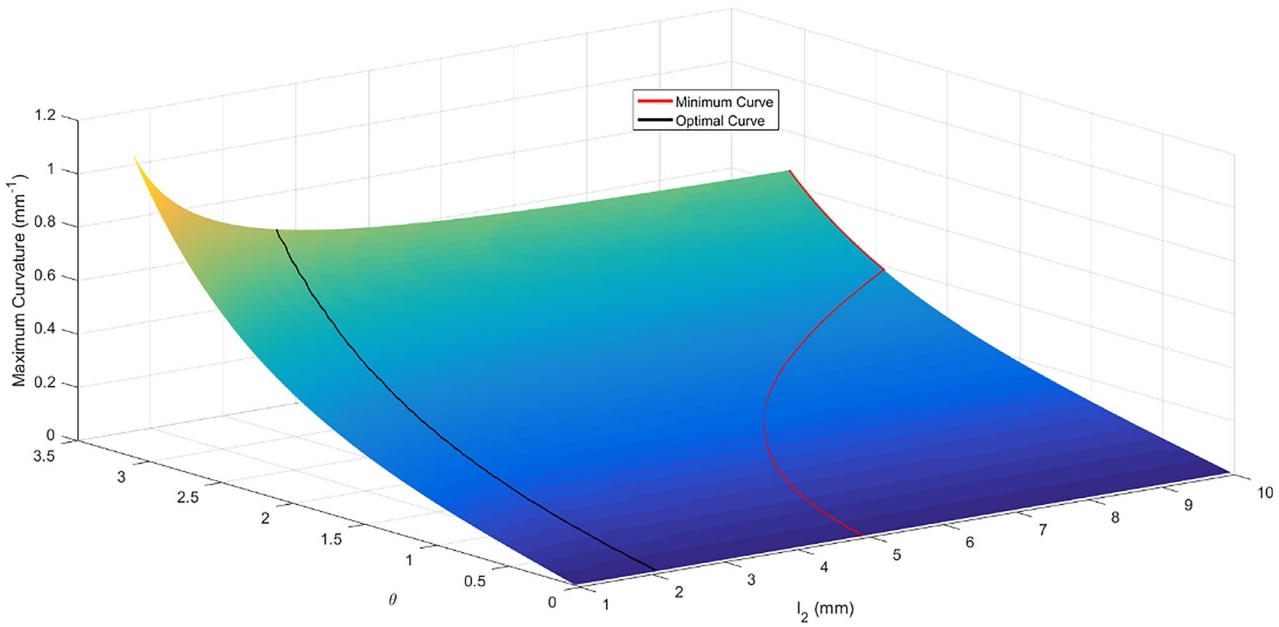

Fig. 3 The curvature extreme of the proposed PH spline with various characteristic length l_2 and the corner angle θ

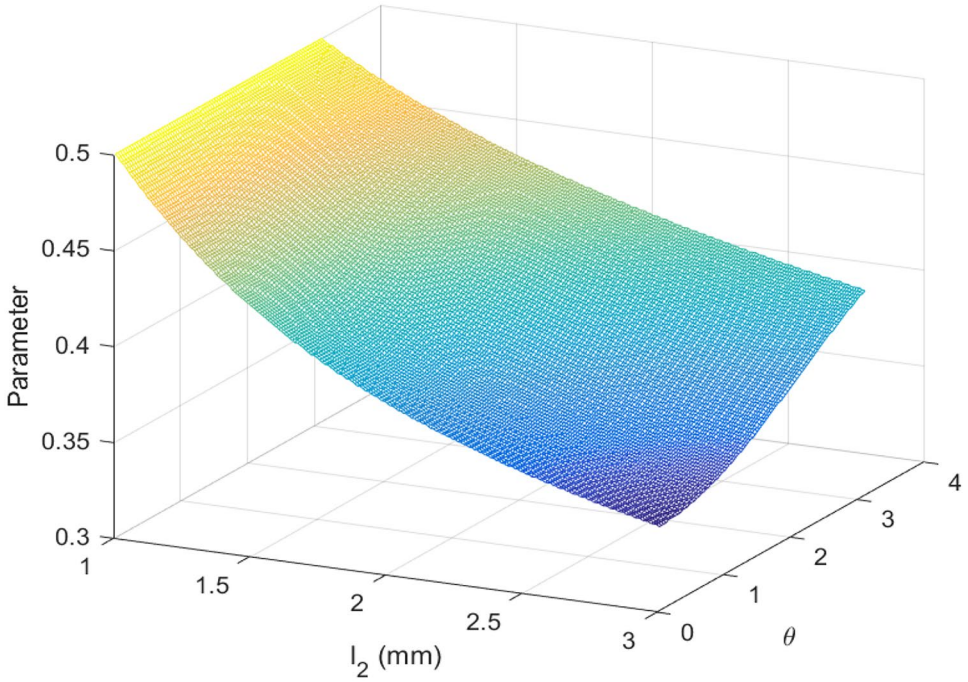

Fig. 4 The parameters of the curvature extreme points on the proposed PH spline with various characteristic length l_2 and the corner angle θ

transition PH spline $R(t)$ as e_R, and the maximal deviation between the linear trajectory $P_0{-}P_1 - P_2$ and the transition PH spline $r(t)$ as e_r, then $e_r \le e_R$.

The proof process of Theorems 3 and 4 can be found in Appendices 3 and 4 respectively. From these two theorems, we get that if $l_1, l_2 \le l_\varepsilon$, then the maximal deviation between the linear trajectory $P_0{-}P_1 - P_2$ and the transition PH spline $r(t)$ satisfies $e_{\max} \le \varepsilon$, where

$$l_\varepsilon = \frac{2^{14}\varepsilon}{sin(\frac{\theta}{2})\left(\frac{4072849}{429} + 714 + \frac{16384\times1225}{858cos(\frac{\theta}{2})}\right)} \tag{14}$$

3.2 Length constraint

In Fig. 5, P_i are $G01$ points, $L_{1,i}$ and $L_{2,i}$ are two transition lengths at point P_i, which can be obtained by

$$\begin{cases} L_{1,i} = \frac{2605}{429} l_{1,i} + \frac{1225}{858\cos\left(\frac{\theta_i}{2}\right)} \sqrt{l_{1,i} l_{2,i}} \\ L_{2,i} = \frac{2605}{429} l_{2,i} + \frac{1225}{858\cos\left(\frac{\theta_i}{2}\right)} \sqrt{l_{1,i} l_{2,i}} \end{cases} \tag{15}$$

where $l_{1,i}$ and $l_{2,i}$ are two characteristic lengths of the transition PH spline at point P_i, and θ_i is the corner angle. Let L_i be the length of linear segment P_iP_{i+1} and n denote the maximum index of $G01$ points (i.e. the $G01$ points are presented by $\{P_0, P_1, \ldots, P_n\}$). To preserve the shape of the toolpath, the sum of two adjacent transition lengths should be less than the linear segment, that is, the following inequalities should be satisfied:

$$\begin{cases} L_{1,1} \le L_0 \\ L_{2,i} + L_{1,i+1} \le L_i i = 1, \ldots, n-2 \\ L_{2,n-1} \le L_{n-1} \end{cases}. \tag{16}$$

From Sect. 2.3, to make full use of the linear lengths, the following equation also needs to be satisfied:

$$max\left(\frac{l_{1,i}}{l_{2,i}}, \frac{l_{2,i}}{l_{1,i}}\right) \le K = 2.5. \tag{17}$$

3.3 The determination of l_1 and l_2 under error constraint and length constraint

In this section, the determination of characteristic lengths l_1 and l_2 for only one corner is given; then, it extends naturally to the toolpath with multiple corners, which is detailed in the next section. For simplicity, denote the corner by linear trajectory $P_0{-}P_1 - P_2$, and the subscript i in Sect. 3.2 is omitted in this section. The error constraint gives $l_1, l_2 \le l_\varepsilon$, where l_ε is calculated by Eq. (14). The length constraint gives $\frac{2605}{429} l_1 + \frac{1225}{858cos\left(\frac{\theta}{2}\right)} \sqrt{l_1 l_2} \le L_b$ and $\frac{2605}{429} l_2 + \frac{1225}{858cos\left(\frac{\theta}{2}\right)} \sqrt{l_1 l_2} \le L_f$, where L_b and L_f are the upper bound of the transition lengths, and $L_b = |P_0P_1|$, $L_f = |P_1P_2|$ for this corner. Combining these inequalities with Eq. (17), the constraint model is as follows:

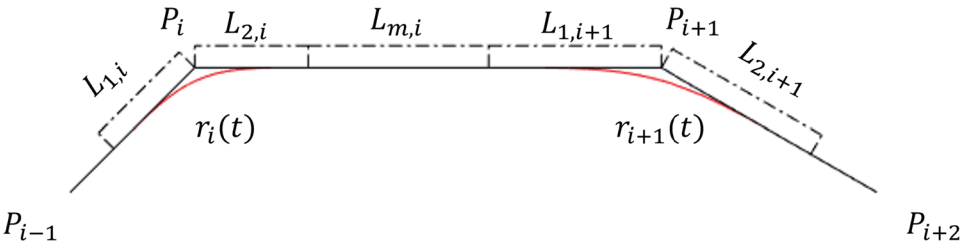

Fig. 5 Length constraint of corner smoothing

$$\begin{cases} k_1 l_1 + k_2\sqrt{l_1 l_2} \le L_b \\ k_1 l_2 + k_2\sqrt{l_1 l_2} \le L_f \\ l_1 \le l_\varepsilon \\ l_2 \le l_\varepsilon \\ max\left(\frac{l_1}{l_2}, \frac{l_2}{l_1}\right) \le K = 2.5 \end{cases} \tag{18}$$

where $k_1 = \frac{2605}{429}$ and $k_2 = \frac{1225}{858\cos(\theta/2)}$.

The goal is to construct a transition spline that satisfies the above constraints and has the smallest curvature extreme. Since the expression of the curvature extreme of the transition spline is too complicated, it is not practical to construct such a transition spline. Considering that the curvature extreme is almost inversely proportional to the characteristic lengths, the goal here is simplified to make the characteristic length as big as possible, which means the first four inequalities in Eq. (18) can take as many equal signs as possible. An algorithm proposed to achieve such a goal is shown below:

Step 1: Let the first two inequalities in Eq. (18) take equal sign; solve this two-dimensional quadratic equations to get l_1 and l_2.
Step 2: If $\frac{l_2}{l_1} > K$, let $l_2 = Kl_1$ and l_1 takes the maximum value that satisfies the first two inequalities in Eq. (18).
Step 3: If $\frac{l_1}{l_2} > K$, let $l_1 = Kl_2$ and l_2 takes the maximum value that satisfies the first two inequalities in Eq. (18).
Step 4: If $l_1, l_2 > l_\varepsilon$, then $l_1 = l_2 = l_\varepsilon$.
Step 5: If $l_1 > l_\varepsilon \ge l_2$, then $l_1 = l_\varepsilon$ and l_2 takes the maximum value that satisfies the first four inequalities in Eq. (18).

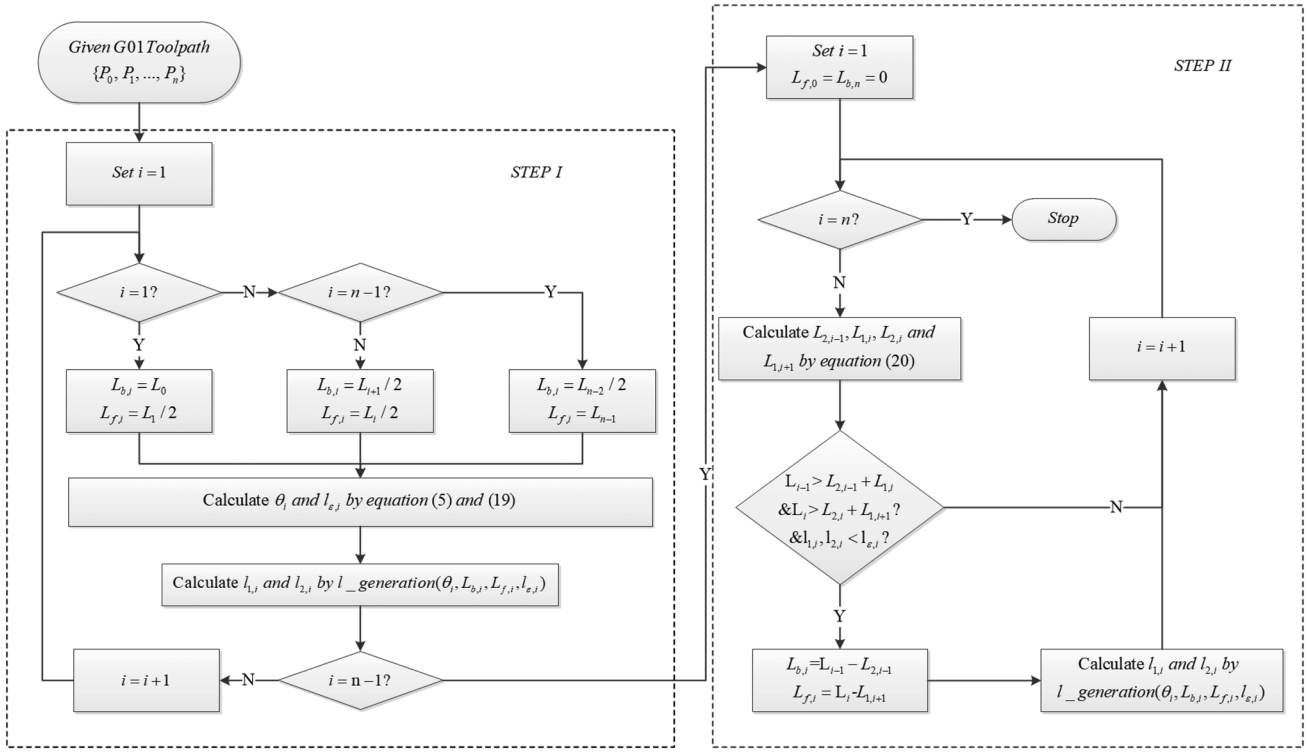

Fig. 6 The flow chart of the proposed method

Step 6: If $l_2 > l_\varepsilon \geq l_1$, then $l_2 = l_\varepsilon$ and l_1 takes the maximum value that satisfies the first four inequalities in Eq. (18).

The pseudocode of this algorithm is also shown as follows:

Algorithm 1

1: $l\_generation(\theta, L_b, L_f, l_\varepsilon)$

2: $k_1 = \frac{2605}{429},\ k_2 = \frac{1225}{858cos(\theta/2)}$

3: $a = k_2^2 - k_1^2,\ b = \frac{(L_f - L_b)k_2^2}{k_1} + 2k_1L_b,\ c = -L_b^2$

4: $l_1 = \frac{-b+\sqrt{b^2-4ac}}{2a},\ l_2 = l_1 + \frac{L_f - L_b}{k_1}$

5: If $\frac{l_2}{l_1} > K = 2.5$ then $l_1 = min\left(\frac{L_b}{k_1+k_2\sqrt{K}}, \frac{L_f}{k_1K+k_2\sqrt{K}}\right),\ l_2 = Kl_1$ end

6: If $\frac{l_1}{l_2} > K = 2.5$ then $l_2 = min\left(\frac{L_b}{k_1K+k_2\sqrt{K}}, \frac{L_f}{k_1+k_2\sqrt{K}}\right),\ l_1 = Kl_2$ end

7: If $l_1 > l_\varepsilon$

8: If $l_2 > l_\varepsilon$ then $l_1 = l_2 = l_\varepsilon$

9: Else $l_1 = l_\varepsilon,\ l_2 = min\left(l_\varepsilon, \frac{(L_b - k_1l_1)^2}{k_2^2l_1}, \frac{(\sqrt{k_2^2l_1+4k_1L_f} - k_2\sqrt{l_1})^2}{4k_1^2}\right)$ end

10: Else if $l_2 > l_\varepsilon$

11: $l_2 = l_\varepsilon,\ l_1 = min\left(l_\varepsilon, \frac{(L_f - k_1l_2)^2}{k_2^2l_2}, \frac{(\sqrt{k_2^2l_2+4k_1L_b} - k_2\sqrt{l_2})^2}{4k_1^2}\right)$

12: End

3.4 Detailed method

For the toolpath presented by $\{P_0, P_1, \ldots, P_n\}$, the C^4 smooth path is generated once the characteristic lengths $l_{1,i}$ and $l_{2,i} (i = 1, 2, \ldots, n-1)$ are determined. From Sect. 3.3, we can see that for the corner at point P_i, the characteristic lengths $l_{1,i}$ and $l_{2,i}$ are determined by the corner angle θ_i, error constraint $l_{\varepsilon,i}$ (which is totally depended on ε and θ_i) and the upper bound of the transition lengths $L_{b,i}$ and $L_{f,i}$. Among these three variables, the first two are fixed; the only one degree of freedom left is the choice of $L_{b,i}$ and $L_{f,i}$, and they are limited by the length constraint, i.e. $L_{b,1} \leq L_0$, $L_{f,i} + L_{b,i+1} \leq L_i (i = 1, \ldots, n-2)$ and $L_{f,n-1} \leq L_{n-1}$.

Our method consists of two steps, where STEP I guarantees that the length constraint will not be violated, and STEP II makes full use of the length of the linear trajectory to make the curvature extreme of the transition curve as small as possible.

STEP I

1. Let the upper bound of the transition lengths equal to the half of the length of the corresponding linear trajectory, i.e. $L_{f,i} = \frac{1}{2}L_i, L_{b,i} = \frac{1}{2}L_{i-1} (i = 1, \ldots, n-1)$. Since the first and the last linear trajectory are not shared by two corners, let $L_{f,n-1} = L_{n-1}, L_{b,1} = L_0$.
2. Calculate θ_i and $l_{\varepsilon,i}$ by Eqs. (5) and (14), and determine $l_{1,i}$ and $l_{2,i}$ by $l\_generation(\theta, L_{b,i}, L_{f,i}, l_{\varepsilon,i})$ for $i = 1, \ldots, n-1$.

STEP II

1. Set i = 1.
2. If $i < n$, calculate the transition lengths $L_{2,i-1}$, $L_{1,i}$, $L_{2,i}$ and $L_{1,i+1}$ by Eq. (15); otherwise, stop.
3. Check whether there exists linear trajectory on the line segment $\overline{P_{i-1}P_i}$ and $\overline{P_iP_{i+1}}$ (see Fig. 5). If $L_{m,i-1}, L_{m,i} > 0$, go to (4); otherwise, go to (6).
4. If $l_{1,i}, l_{2,i} < l_{\varepsilon,i}$, the characteristic lengths of the transition PH spline can be increased, go to (5); otherwise, go to (6).
5. Let $L_{b,i} = L_{i-1} - L_{2,i-1}$ and $L_{f,i} = L_i - L_{1,i+1}$; update $l_{1,i}$ and $l_{2,i}$ by $l\_generation(\theta, L_{b,i}, L_{f,i}, l_{\varepsilon,i})$.

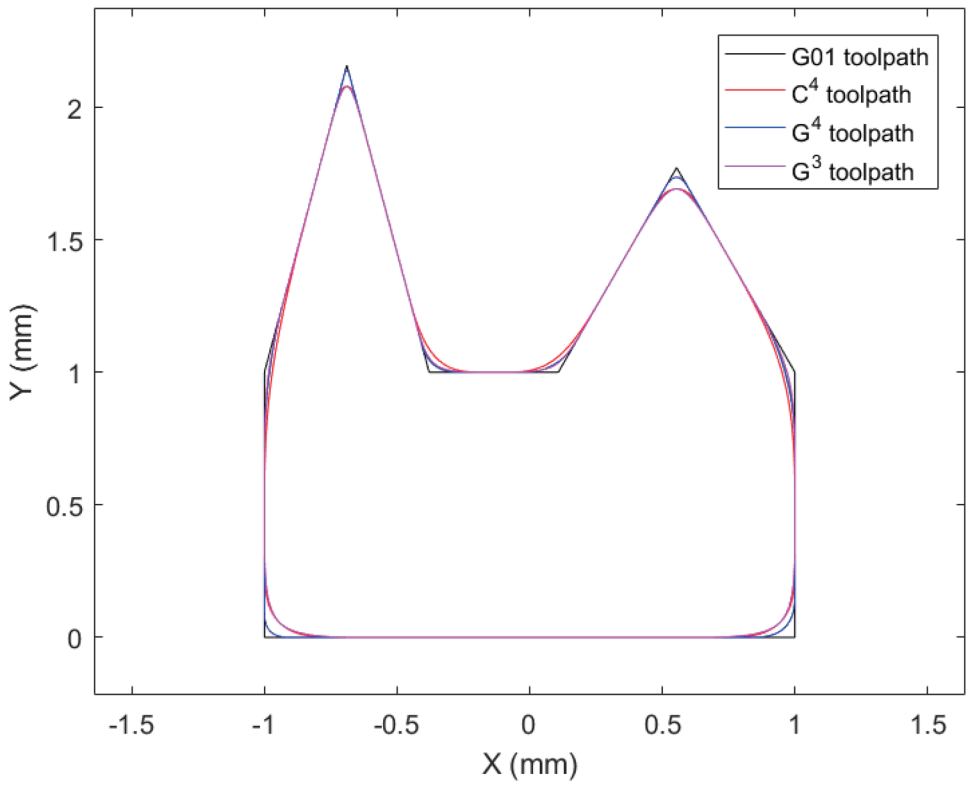

Fig. 7 A polygonal shape *G*01 toolpath and its three smooth paths

6. $i = i + 1$, go to (2).

The flow chart of the proposed method is illustrated in Fig. 6.

3.5 A simple case

To demonstrate the advantages of our corner smoothing method, our method and other two B-spline based methods in [3] (denoted by G^4 method) and [18] (denoted by G^3 method) are applied to the same *G*01 toolpath, which is shown as Fig. 7. To show the geometric properties of the three smooth paths generated by these methods, the curves with the arc length as the abscissa value and the curvature value as the ordinate value corresponding to it are shown in Fig. 8. Compared with G^3 method and G^4 method, the curvature extreme has been decreased by 59.63% and 86.14%, and the arc length has been decreased by 0.25% and 3.33%. In most cases, the smaller arc length and curvature extreme will lead to shorter machining time. To further verify whether our method can reduce the machining time, a feedrate scheduling scheme is introduced in Sect. 4, and the simulation is shown in Sect. 5.

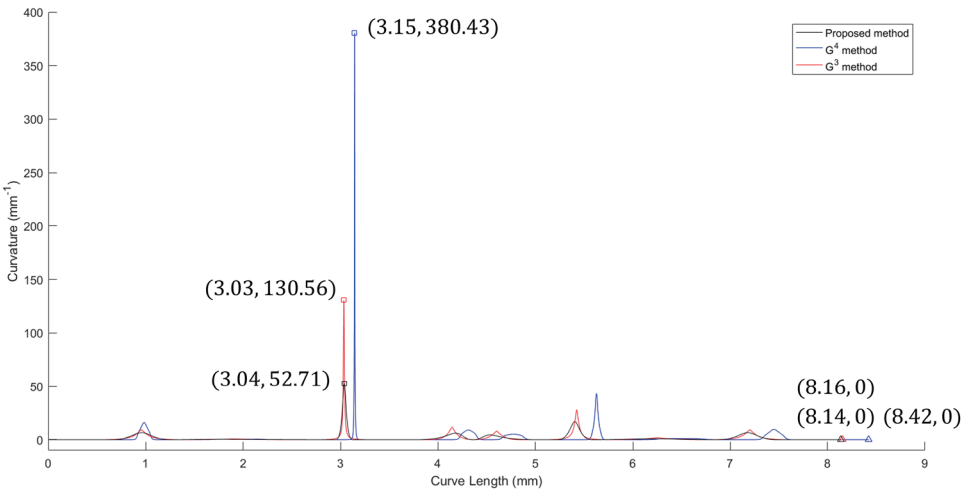

Fig. 8 Curvature as a function of arc length for these three smoothing algorithms

4 Feedrate planning of C^4 smooth path

In this section, the critical points of the smooth path and their maximum allowable feedrate are determined first; then, the division of the smooth path is presented, and the jerk-continuous feedrate scheduling scheme in Ref. [32] is adopted finally.

4.1 Determination of critical points and their feedrate

When planning the feedrate along a PH spline, the chord error, centripetal acceleration and jerk limitations should be taken into account. From Ref. [31], the maximum allowable feedrate can be calculated by

$$v_m = min(F, \frac{2}{T_s}\sqrt{\frac{2\delta}{k} - \delta^2}, \sqrt{\frac{A_n}{k}}, \sqrt[3]{\frac{J_n}{k^2}}) \tag{19}$$

where F is the command feedrate, T_s is the interpolation period, k is the curvature, δ is the chord error limitation, A_n and J_n are the acceleration and jerk limitations respectively. From Eq. (19), the local minimum feedrate occurs at the local curvature extreme points of the smooth path, which are also the curvature extreme points of all inserted PH splines. However, the parameter of the curvature extreme point of the inserted PH spline cannot be given analytically because the PH spline is asymmetric. Instead, the bilinear interpolation method is applied to estimate the parameters of the curvature extreme points.

For an inserted PH spline, assuming its characteristic lengths are l_1 and l_2, and the corresponding corner angle is θ. The parameter of the curvature extreme point of this inserted PH spline is determined as follows:

Step 1: Define the ratio of the two characteristic lengths as $R_{1,2} = max(\frac{l_1}{l_2}, \frac{l_2}{l_1})$, and let $i = \lfloor 180 \times \theta/\pi \rfloor$ and $j = \lfloor R_{1,2}/0.01 \rfloor$.

Step 2: According to matrix M in Sect. 2, denote four close parameters of the curvature extreme point as $t_{0,0} = M(i+1, j-99)$, $t_{1,0} = M(i+2, j-99)$, $t_{0,1} = M(i+1, j-98)$ and $t_{1,1} = M(i+2, j-98)$.

Step 3: Apply bilinear interpolation method to estimate the parameter as $t_m = (1-x)(1-y)t_{0,0} + x(1-y)t_{1,0} + (1-x)yt_{0,1} + xyt_{1,1}$, where $x = \frac{180\theta}{\pi} - i$ and $y = 100R_{1,2} - j$.

Step 4: Let $t_{\max} = \max(t_{0,0}, t_{1,0}, t_{0,1}, t_{1,1})$, $t_{\min} = \min(t_{0,0}, t_{1,0}, t_{0,1}, t_{1,1})$, $n_1 = \lfloor 1000 t_{\min} \rfloor$ and $n_2 = \lceil 1000 t_{max} \rceil$. Determine a parameter set as $\left\{ t_a | t_a = \frac{a+n_1}{1000}, a = 0, 1, 2, \ldots, n \right\}$, where $n = n_2 - n_1$.

Step 5: If $l_1 > l_2$, let $t_m = 1 - t_m$ and $t_a = 1 - t_a$ for $a = 0, 1, 2, \ldots, n$.

Step 6: Calculate the curvature of the inserted PH spline at parameter t_m and $t_a (a = 0, 1, 2, \ldots, n)$, and denote them as k_m and k_a. Let $k_{\max} = \max(k_m, k_a)$ and t_m equals to the parameter whose curvature is $k_{\max}$.

The critical point of this PH spline can be obtained by substituting t_m into the parametric equation $r(t)$, and the maximum allowable feedrate can be calculated by Eq. (19).

4.2 The division of the smooth path

For the toolpath presented by $\{P_0, P_1, \ldots, P_n\}$, denote the inserted PH spline at point P_i as $r_i(t) (i = 1, 2, \ldots, n-1)$. The parameter of the curvature extreme point of $r_i(t)$ and its maximum allowable feedrate can be obtained by the bilinear interpolation method in Sect. 4.1, which are denoted as t_i and v_i respectively. Then, the smooth path is split into n blocks based on the critical points $r_i(t_i)$.

The first block contains the remainder of the first linear segment and part of $r_1(t)$. The start point and end point of this block are P_0 and $r_1(t_1)$, the start velocity and end velocity of this block are 0 and v_1 and the length of this block can be calculated as follows:

$$S_1^b = l_1^r + s_1(t_1) \tag{20}$$

Table 1 The parameters used in simulation

Parameters	Constraints	Symbols	Values	Units
Smoothing parameters	Transition error	ε	0.08	mm
	Ratio threshold	K	2.5	none
Machining parameters	Command feedrate	F	200	mm/s
	Tangential acceleration	A_t	3000	mm/s^2
	Centripetal acceleration	A_n	3000	mm/s^2
	Tangential jerk	J_t	60000	mm/s^3
	Centripetal jerk	J_n	60000	mm/s^3
	Chord error	δ	0.001	mm
	Interpolation period	T_s	1	ms

where l_1^r is the length of the remainder of the first linear segment, $s_1(t)$ is the cumulative arc length function of $r_1(t)$, which can be obtained by Eq. (3).

The $ith (i = 2, 3, \ldots, n-1)$ block contains part of $r_{i-1}(t)$, the remainder of the *ith* linear segment and part of $r_i(t)$. The start point and end point of this block are $r_{i-1}(t_{i-1})$ and $r_i(t_i)$, the start velocity and end velocity of this block are v_{i-1} and v_i and the length of this block can be calculated as follows:

$$S_i^b = (s_{i-1}(1) - s_{i-1}(t_1)) + l_i^r + s_i(t_i) \tag{21}$$

where l_i^r is the length of the remainder of the *ith* linear segment, and s_i(t) is the cumulative arc length function of $r_i(t)$.

The last block contains part of $r_{n-1}(t)$ and the remainder of the last linear segment. The start point and end point of this block are $r_{n-1}(t_{n-1})$ and P_n, the start velocity and end velocity of this block are v_{n-1} and 0 and the length of this block can be calculated as follows:

$$S_n^b = (s_{n-1}(1) - s_{n-1}(t_{n-1})) + l_n^r \tag{22}$$

where l_n^r is the length of the remainder of the *nth* linear segment, and s_i(t) is the cumulative arc length function of $r_i(t)$.

It is worth noting that the remainder of linear segment may degenerate into a point when it is completely replaced by two adjacent inserted PH splines. At this time, l_i^r in Eqs. (20–22) equals to 0, which will not have an essential effect on the division of the smooth path.

4.3 The jerk-continuous feedrate scheduling scheme

Since the start and end velocity of blocks are obtained only considering the chord error limitation, the acceleration limitation and the jerk limitation, when the length is too short, the feedrate may not be able to smoothly transition from the start velocity to the end velocity. To guarantee the continuity of the feedrate at the junctions between successive blocks, the bidirectional scanning module in [32] is applied to adjust the start velocity and the end velocity if necessary. Then, the velocity scheduling module in [32] is used to plan the feedrate along every block. Combining the feedrate along every block together, a jerk-continuous feedrate profile along the C^4 smooth path is obtained.

5 Simulation results

In this section, the proposed corner smoothing method is validated by three different types of toolpaths. As a comparison, other two B-spline based methods in [18] (denoted by G^3 method) and [3] (denoted by G^4 method) are also applied to the same toolpaths. After the toolpaths are rounded by different smoothing methods, the feedrate scheduling scheme

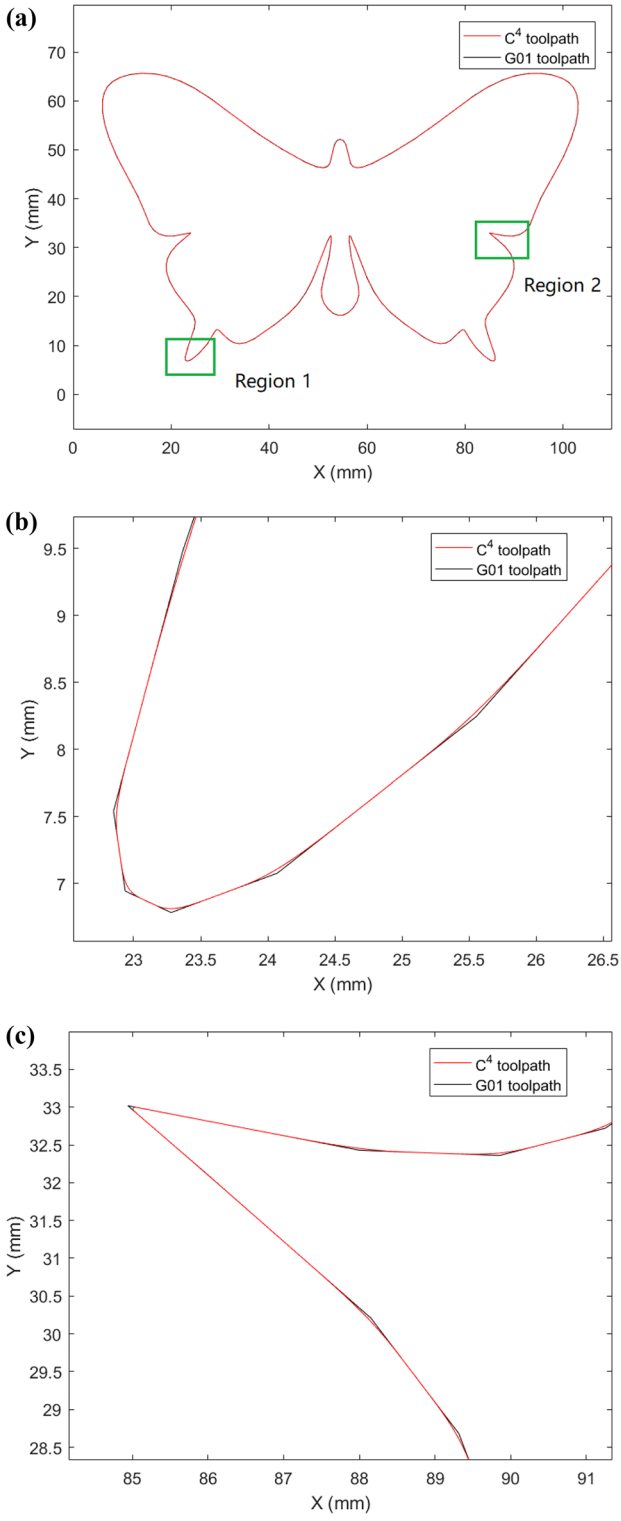

Fig. 9 Butterfly-shaped toolpath with C^4 continuity. (**a**) Toolpath smoothing. (**b**) Detailed result of region 1. (**c**) Detailed result of region 2

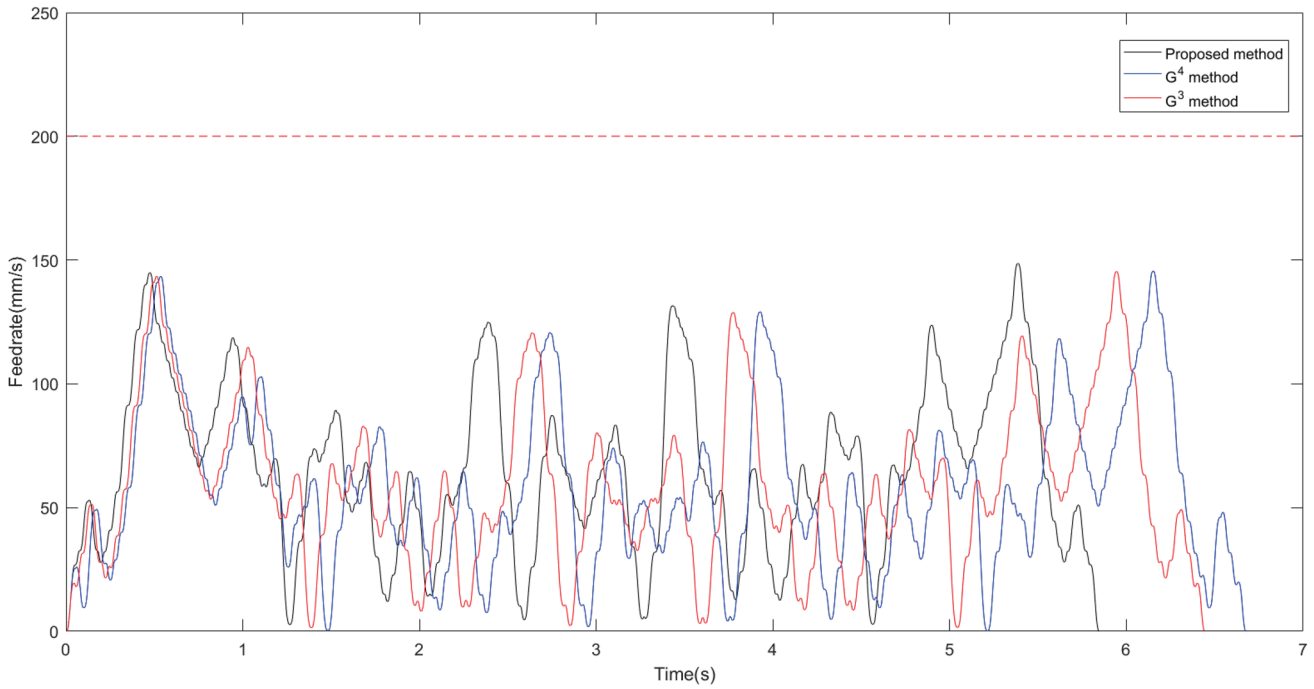

Fig. 10 The feedrate profiles of butterfly-shaped toolpath compared with G^4 method and G^3 method

in Sect. 4 is proposed to interpolate the smooth paths. Then, the contour errors, feedrate, acceleration and jerk profiles are analyzed to compare the above three smoothing methods in machining quality and efficiency. The related parameters used in this section are listed in Table 1.

5.1 Simulation 1

In this section, a 2D NURBS curve named butterfly-shaped curve is discretized to linear segments as a toolpath to evaluate the performance of the proposed corner

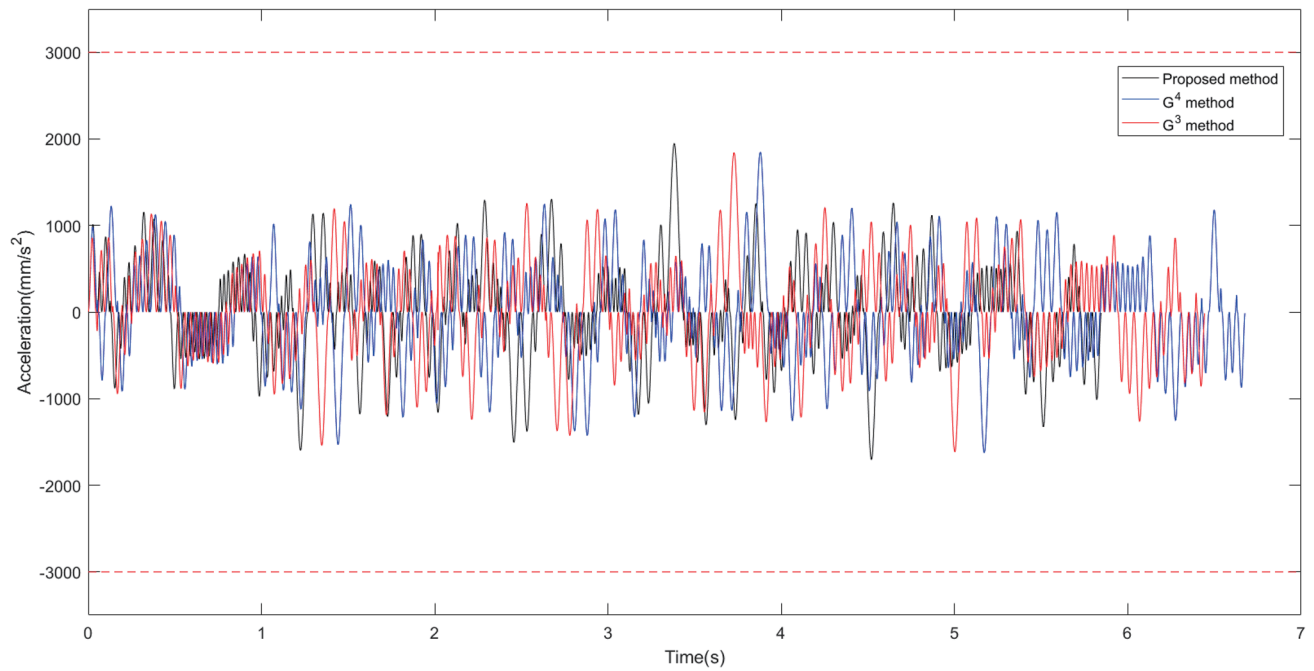

Fig. 11 The acceleration profiles of butterfly-shaped toolpath compared with G^4 method and G^3 method

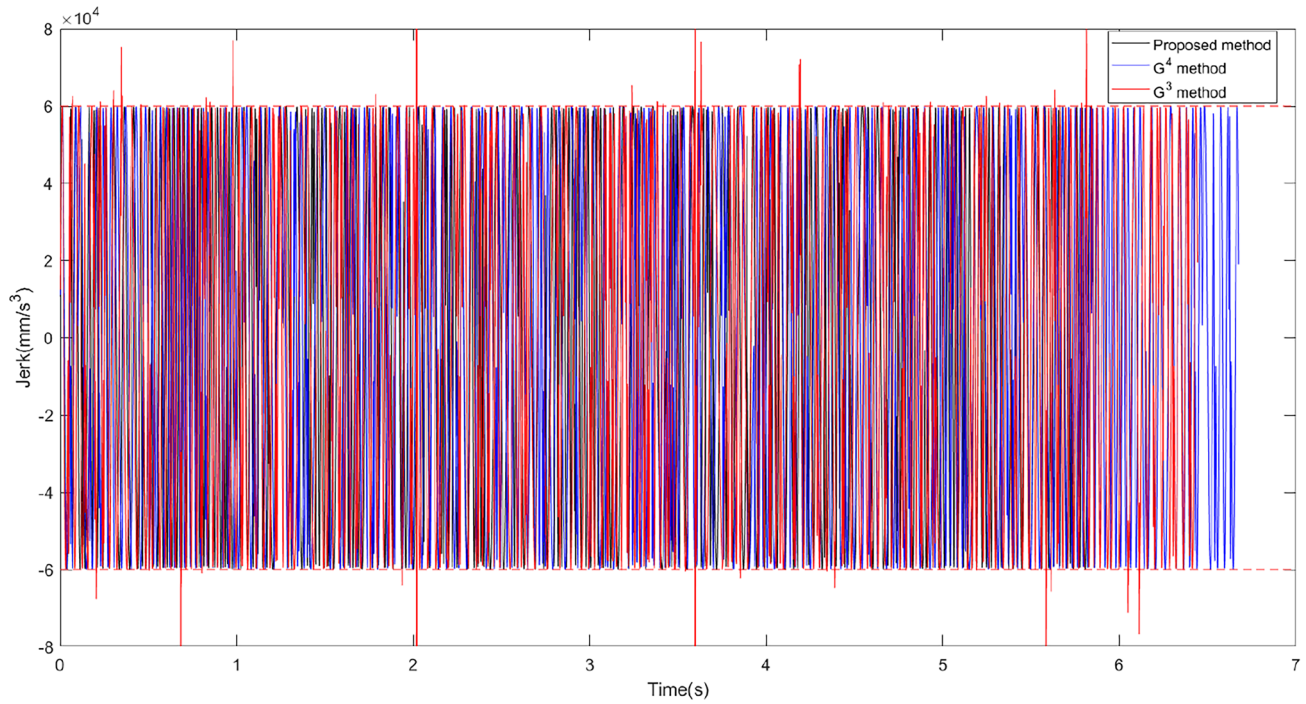

Fig. 12 The jerk profiles of butterfly-shaped toolpath compared with G^4 method and G^3 method

smoothing method. The degrees, control points, knot vectors and weight vectors of butterfly-shaped curve are given in Appendix 5.

As shown in Fig. 9, the linear trajectories near the corners are replaced by PH splines, which makes the toolpath C^4 continuous. To clearly illustrate the generated corner

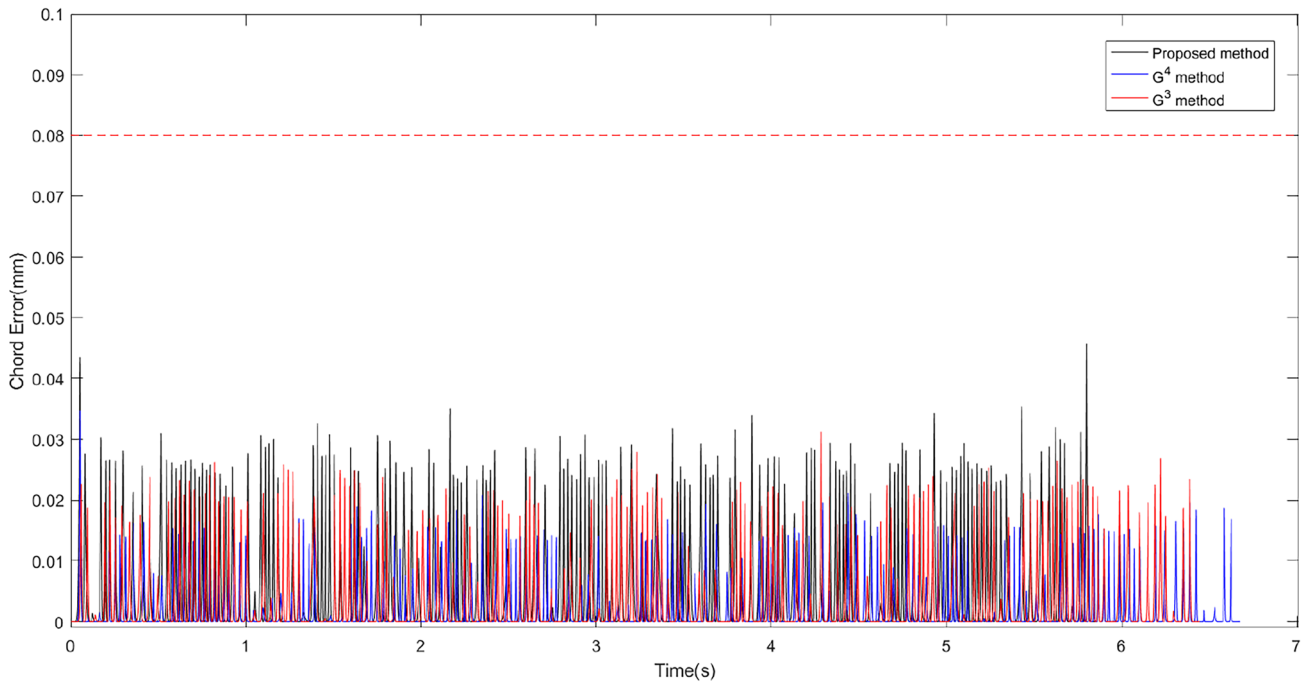

Fig. 13 The chord errors profiles of butterfly-shaped toolpath compared with G^4 method and G^3 method

Table 2 The machining times of butterfly-shaped toolpath under different constraints

F	$A = \frac{1500\text{mm}}{\text{s}^2}$						$A = \frac{3000\text{mm}}{\text{s}^2}$					
	$J = \frac{60{,}000\text{mm}}{\text{s}^3}$			$J = \frac{120{,}000\text{mm}}{\text{s}^3}$			$J = \frac{60{,}000\text{mm}}{\text{s}^3}$			$J = 120{,}000\text{mm/s}^3$		
100**mm/s**	6.210 base	6.947 ↑ 11.87%	6.721 ↑ 8.23%	5.537 base	6.168 ↑ 11.39%	6.016 ↑ 8.65%	6.046 base	6.835 ↑ 13.05%	6.609 ↑ 9.31%	5.126 base	5.694 ↑ 11.08%	5.528 ↑ 7.84%
200**mm/s**	6.038 base	6.832 ↑ 13.15%	6.596 ↑ 9.24%	5.190 base	5.929 ↑ 14.24%	5.752 ↑ 8.28%	5.848 base	6.678 ↑ 14.19%	6.445 ↑ 10.21%	4.659 base	5.322 ↑ 14.23%	5.128 ↑ 10.07%

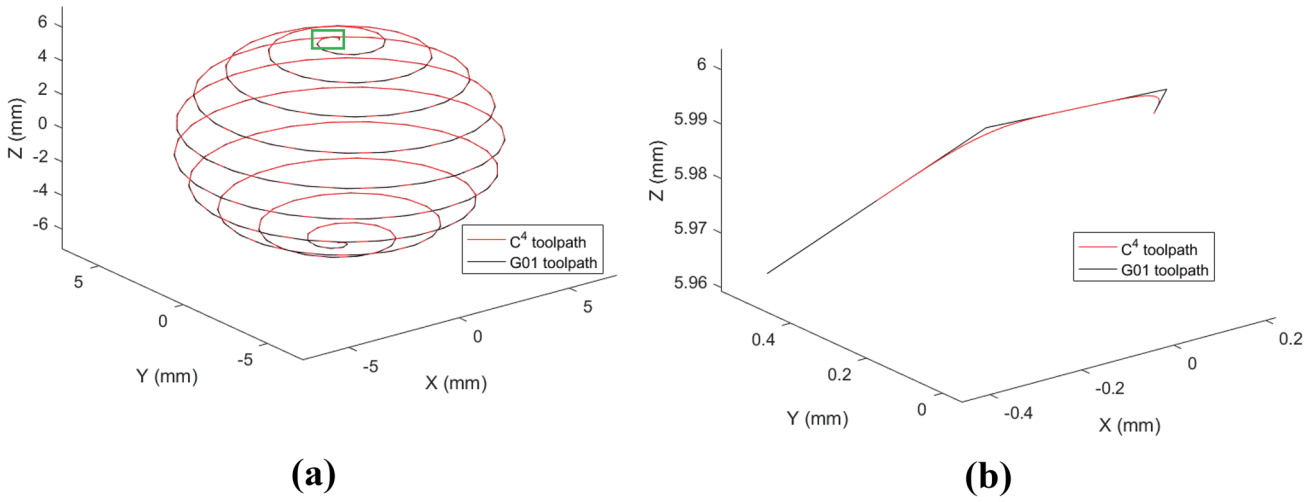

Fig. 14 Spherical helix toolpath with C^4 continuity. (**a**) Toolpath smoothing. (**b**) Detailed result

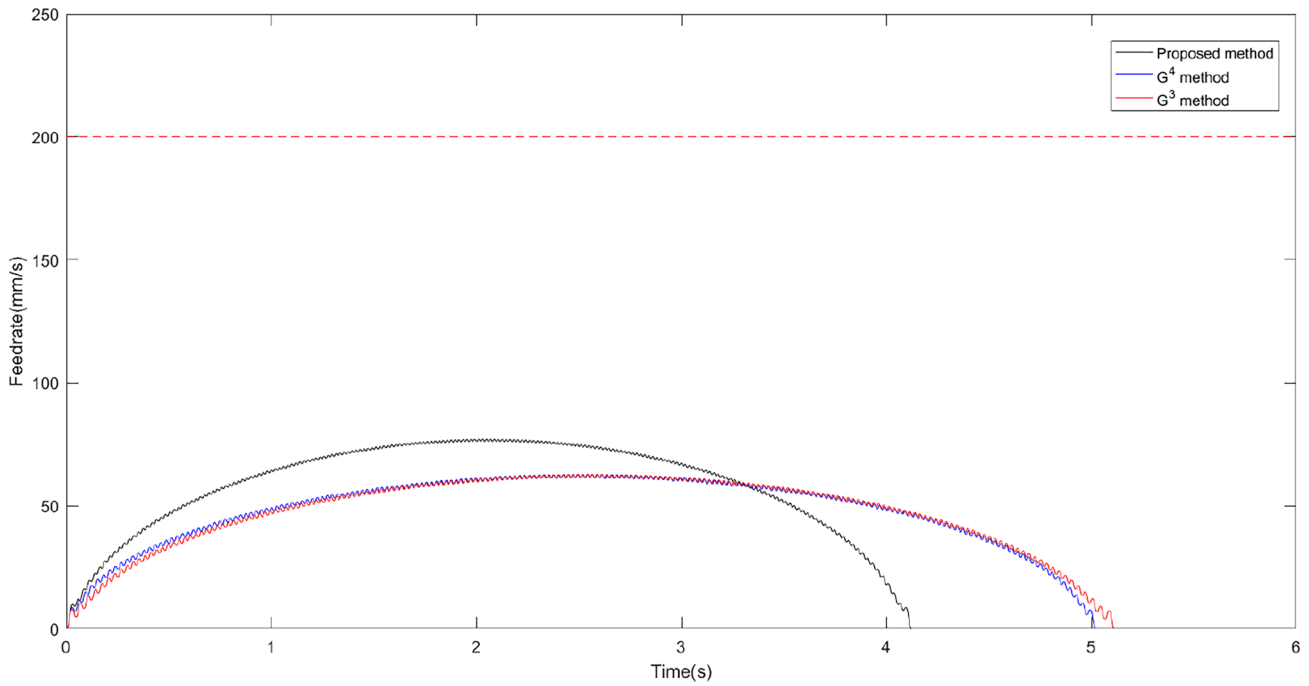

Fig. 15 The feedrate profiles of spherical helix toolpath compared with G^4 method and G^3 method

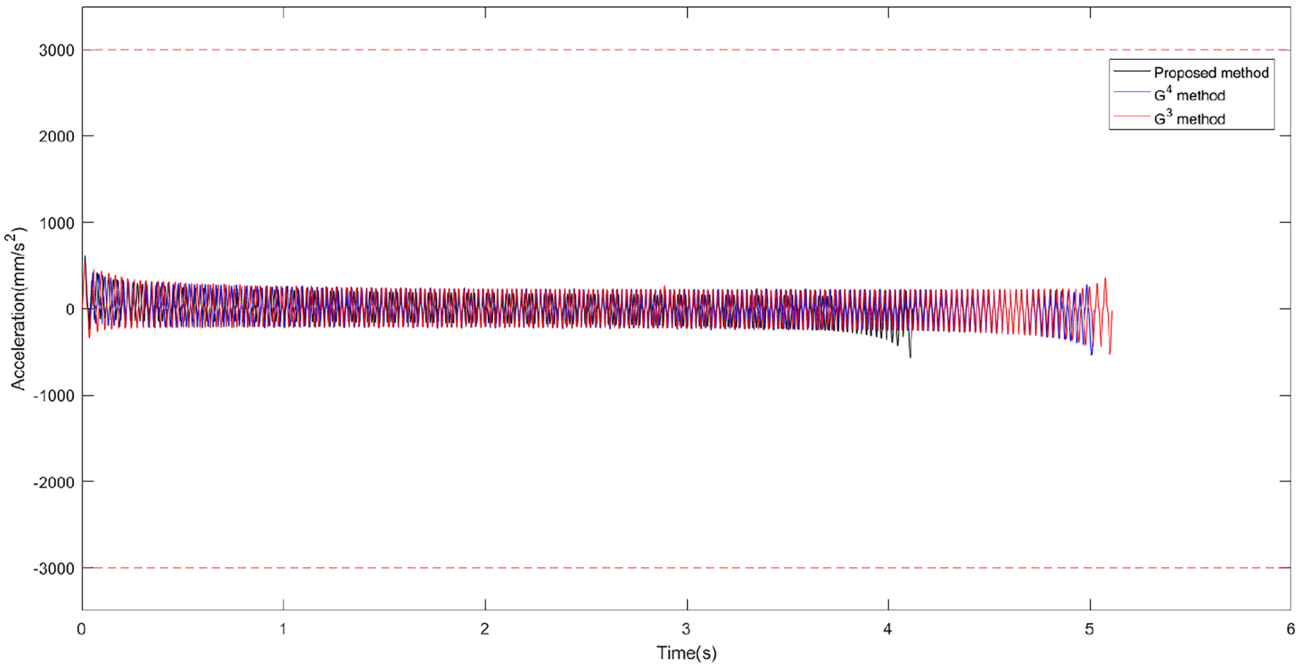

Fig. 16 The acceleration profiles of spherical helix toolpath compared with G^4 method and G^3 method

transition curve, two regions are enlarged as shown in Fig. 9b, c. The feedrate, acceleration, jerk and chord errors profiles of the proposed method, G^4 method and G^3 method can be calculated by interpolation points, which are presented in Figs. 10, 11, 12 and 13.

From Figs. 10 and 11, the feedrate and acceleration are all subjected to the given limitations. However, it can be noted from Fig. 12 that the jerk profile of G^3 method excesses the maximum allowable jerk in some interpolating points, which will lead to violent vibration of the machine

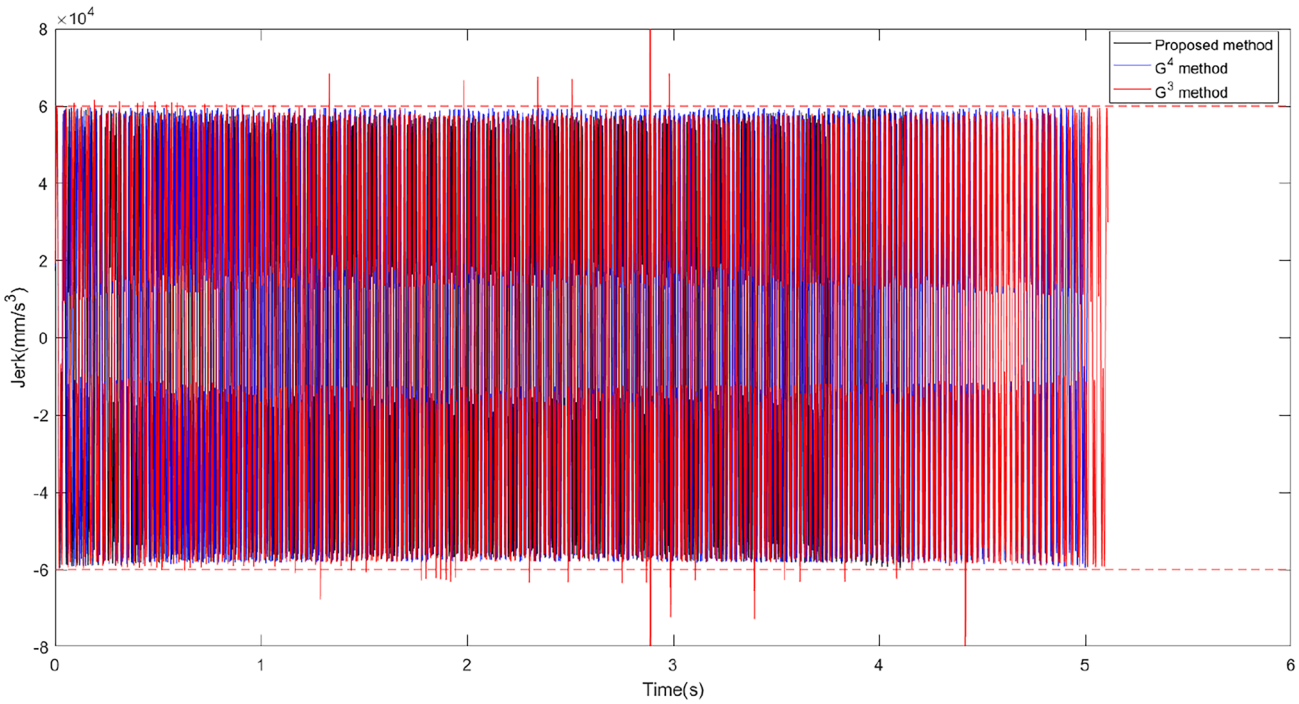

Fig. 17 The jerk profiles of spherical helix toolpath compared with G^4 method and G^3 method

tool, and the machining quality will be affected. As can be seen from Fig. 13, although the chord errors of the proposed method are larger than G^4 method and G^3 method, they are all smaller than the given threshold, so the machining quality is not significantly affected.

In machining efficiency, the machining time of these three different methods are 5.848s, 6.678s and 6.445s respectively. The machining time of the proposed method is 12.43% shorter than G^4 method and 9.26% shorter than G^3 method, which means the proposed method can improve the machining efficiency when the machining parameters are set as in Table 1. To further validate the machining efficiency of the proposed method, the machining time of these three different methods when the feedrate, tangential acceleration, centripetal acceleration, tangential jerk and centripetal jerk constraints take different values are calculated and compared. As listed in Table 2, based on the machining time of the proposed method, the machining time of G^4 method and G^3 method has increased by 7.84% to 14.24%. In other words, the machining efficiency can be improved by the proposed method under different constraints.

5.2 Simulation 2

In this section, a 3D parametric curve named spherical helix curve is discretized to linear segments as a toolpath to evaluate the performance of the proposed corner smoothing method. The parametric equation of this curve is given as follows:

$$\begin{cases} x = 6sin(\theta)cos(\varphi) \\ y = 6sin(\theta)sin(\varphi) \\ z = 6cos(\theta) \end{cases} \tag{23}$$

where $\theta = \pi t$, $\varphi = 20\pi t$ and $t \in [0, 1]$.

From Figs. 14, 15, 16, 17 and 18, in terms of machining quality of spherical helix toolpath, we can get the same conclusion as in Simulation 1. However, in machining efficiency, the machining time of these three different methods are 4.125s, 5.022s and 5.114s respectively. The machining time of the proposed method is 17.86% shorter than G^4 method and 19.34% shorter than G^3 method. As listed in Table 3, based on the machining time of the proposed method, the machining time of G^4 method and G^3 method has increased by 15.49% to 23.98%. It is worth noting that compared with G^4 method and G^3 method, the proposed method has a greater improvement in machining efficiency of spherical helix toolpath than butterfly-shaped toolpath. The reason is that the linear segments of spherical helix toolpath change more frequently in direction and length, so that the advantages of the asymmetry of the proposed method can be fully utilized.

5.3 Simulation 3

In this section, a compound freeform surface composed of two NURBS patches, which presented in Fig. 19, is tested. The toolpath of this freeform surface is generated by Su's

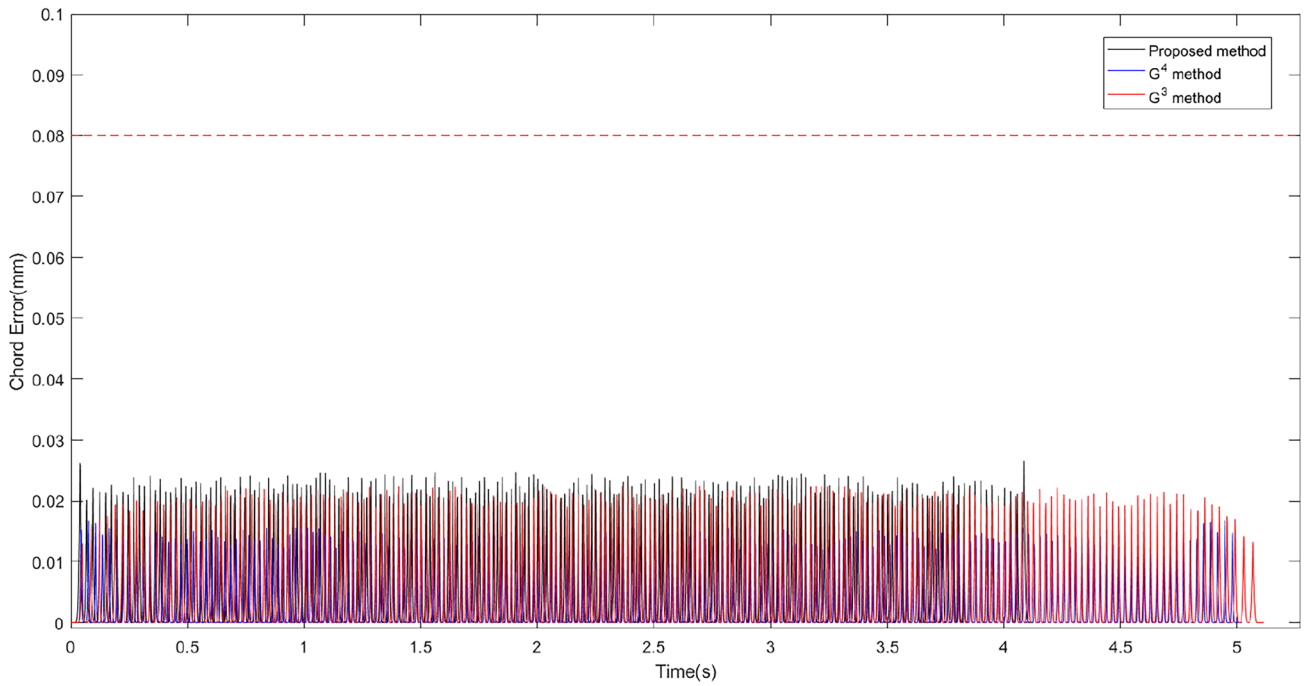

Fig. 18 The chord errors profiles of spherical helix toolpath compared with G^4 method and G^3 method

Table 3 The machining times of spherical helix toolpath under different constraints

F	$A = 1500\mathbf{mm/s}^2$						$A = 3000\mathbf{mm/s}^2$					
	$J = \frac{60{,}000\mathbf{mm}}{s^3}$			$J = \frac{120{,}000\mathbf{mm}}{s^3}$			$J = \frac{60{,}000\mathbf{mm}}{s^3}$			$J = 120{,}000\mathbf{mm}/s^3$		
100**mm/s**	4.599	5.367	5.455	4.474	5.167	5.232	4.125	5.022	5.114	3.357	3.991	4.064
	base	↑ 16.70%	↑ 18.61%	base	↑ 15.49%	↑ 16.94%	base	↑ 21.75%	↑ 23.98%	base	↑ 18.89%	↑ 21.06%
200**mm/s**	4.599	5.367	5.455	4.474	5.167	5.232	4.125	5.022	5.114	3.357	3.991	4.064
	base	↑ 16.70%	↑ 18.61%	base	↑ 15.49%	↑ 16.94%	base	↑ 21.75%	↑ 23.98%	base	↑ 18.89%	↑ 21.06%

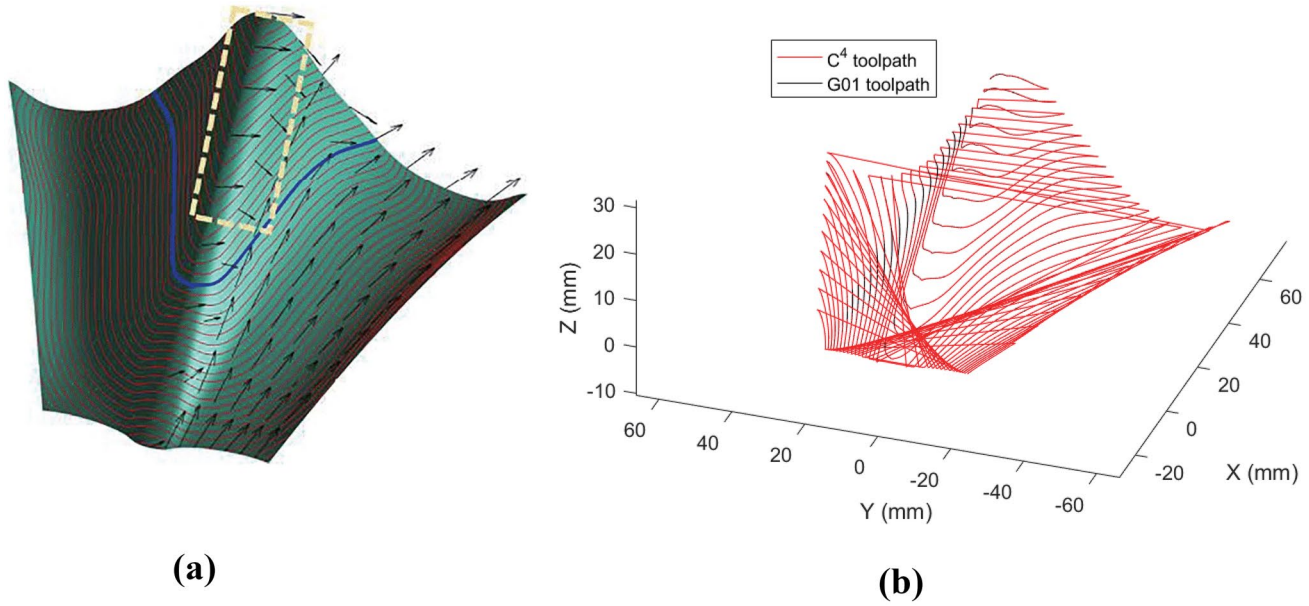

Fig. 19 A compound freeform surface. (**a**) Surface. (**b**) Toolpath

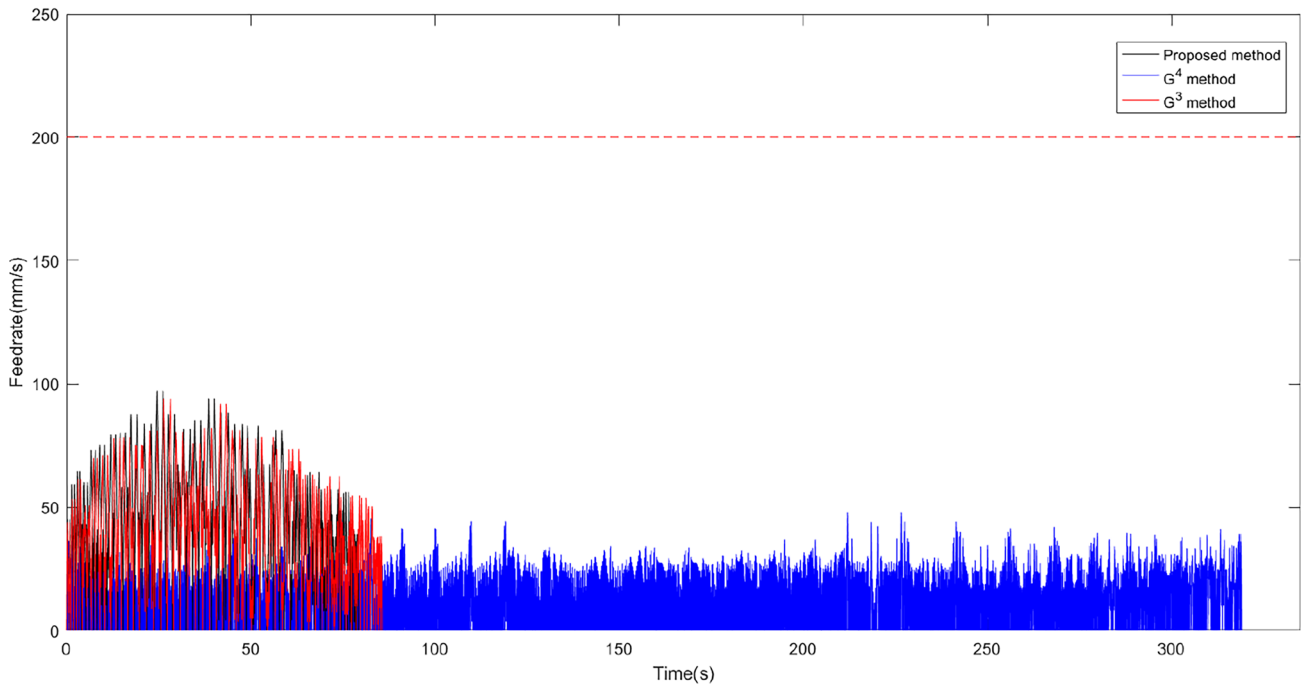

Fig. 20 The feedrate profiles of freeform surface toolpath compared with G^4 method and G^3 method

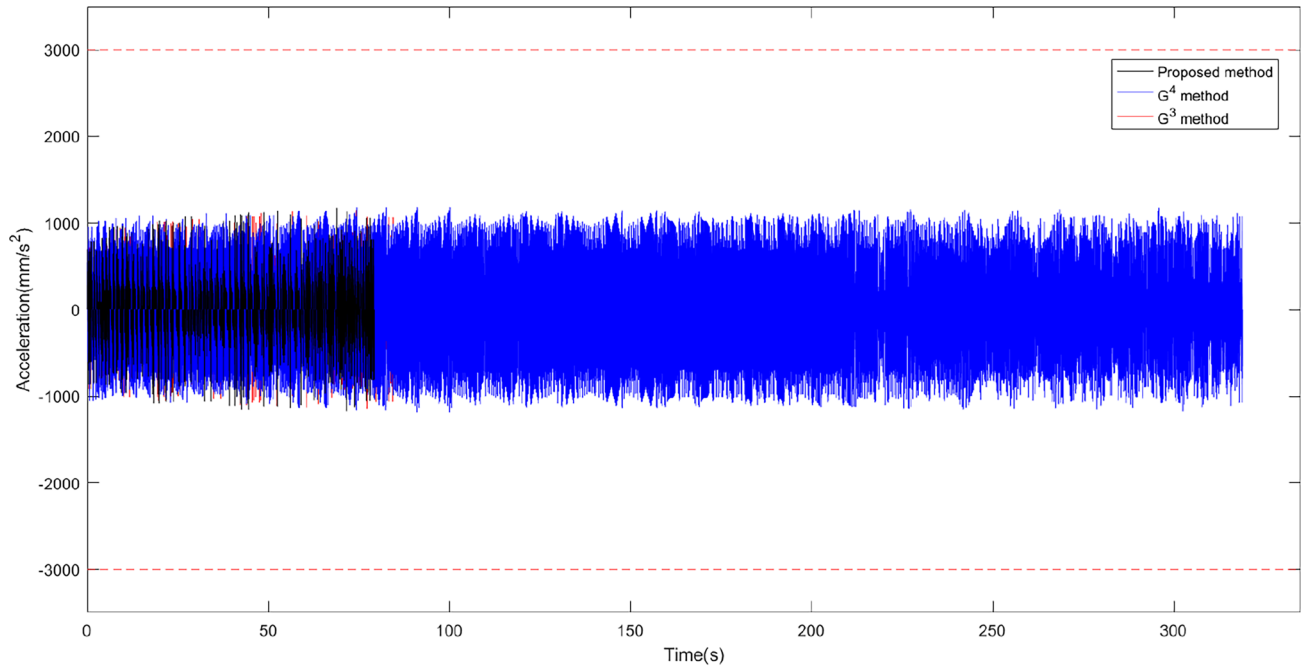

Fig. 21 The acceleration profiles of freeform surface toolpath compared with G^4 method and G^3 method

method [33], which is composed of 58 linear toolpaths with corner points number ranging from 32 to 224. The transition error is 0.02mm and other related parameters are the same as in Table 1.

It can be seen from Figs. 19, 20, 21 and 22, for the toolpath of freeform surface, the proposed method can replace the sharp corners with transition curves and generate smooth velocity, acceleration, jerk profiles whose extremes do not

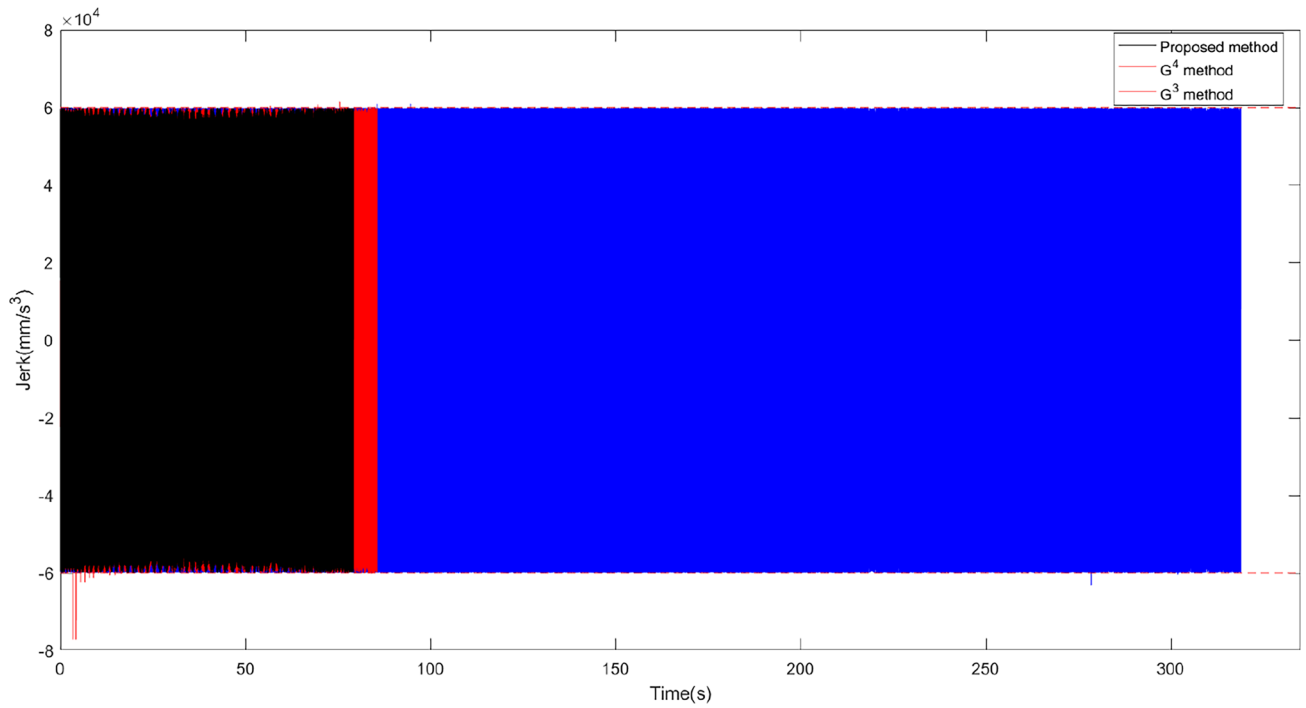

Fig. 22 The jerk profiles of freeform surface toolpath compared with G^4 method and G^3 method

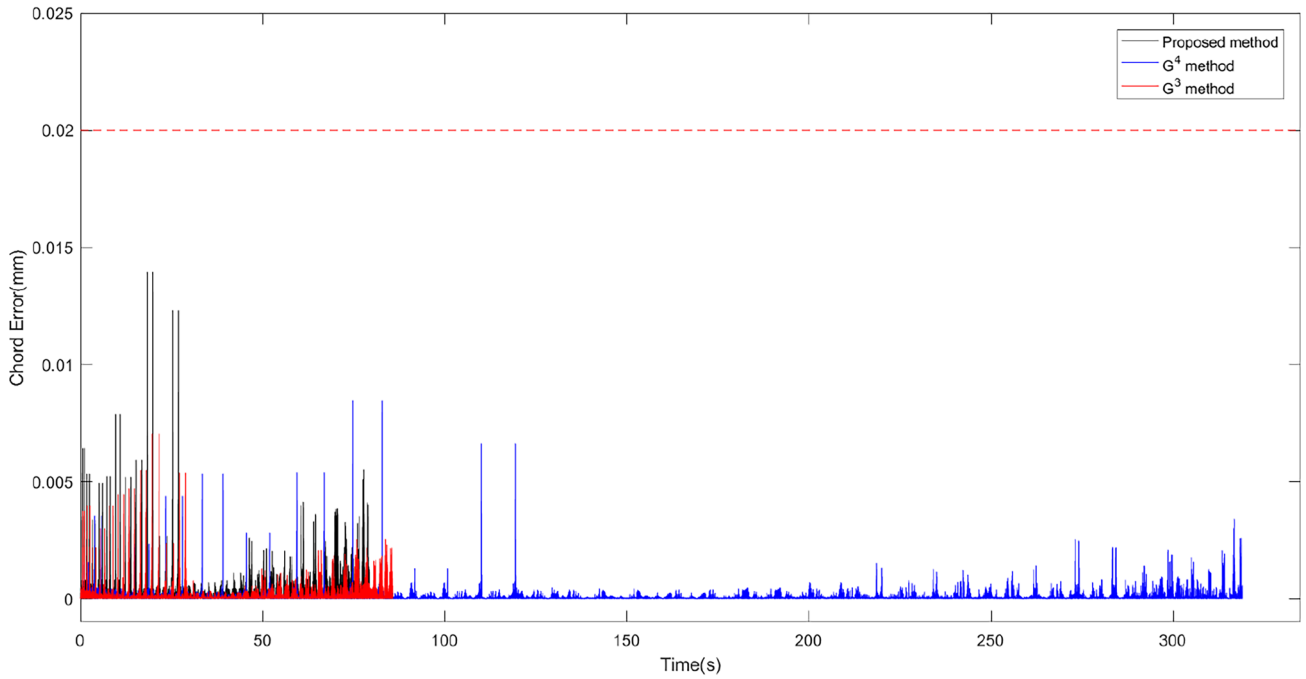

Fig. 23 The chord error profiles of freeform surface toolpath compared with G^4 method and G^3 method

exceed the given limitations, while the jerk extreme of G^4 method and G^3 method excesses the maximum allowable jerk in some interpolating points, which will affect the machining quality. From Fig. 23, although the chord errors of the proposed method are larger than G^3 method and G^4 method, they are all subjected to the given limitations, so the machining quality is not significantly affected.

In machining efficiency, the machining time of these three different methods are 79.436s, 319.090s and 85.860s respectively. The machining time of the proposed method is 75.11% shorter than G^4 method and 7.48% shorter than G^3 method. It can be noted that in the previous two simulations, the machining time of the proposed method, G^3 method and G^4 method are similar. However, in this simulation, the machining time of G^4 method is much higher than the other two methods. Actually, in the order of magnitude, it is closer to the machining time of point-to-point method, which is 545.177s. The reason is that the toolpath of the freeform surface consists of a large number of dense and short linear segments, while G^4 method requires longer transition lengths for the same transition error, which makes the curvature extreme at the corners larger, so that the maximum allowable velocity at the corners is close to zero. From the previous two simulations, it can be seen that the proposed method is more efficient than G^3 method and G^4 method; even the feedrate, tangential acceleration, centripetal acceleration, tangential jerk and centripetal jerk constraints take different values, so only the cases with the same parameters as in Table 1 are compared.

6 Conclusions and future work

This study presents a novel local corner transition method based on asymmetrical C^4 continuous PH spline curve and a jerk-continuous feedrate scheduling scheme. Due to the asymmetry of PH spline curve, the construction of transition curve is more flexible. Although the asymmetry leads to unanalytical curvature extreme and corresponding parameter, a matrix M which stored the parameters of curvature extreme points of different PH spline curves can be pre-calculated to solve this problem.

Advantages of our method are summarized as follows:

a. The corner transition method guarantees the curvature continuity, C^4 continuity and maximum transition error of the smoothed toolpath. Furthermore, the cumulative arc length is a polynomial with respect to parameter of the transition curve, which makes the calculation of interpolation points more efficient.
b. The curvature extreme of the smoothed toolpath is greatly reduced. Compared with two existing method, it has been decreased by 59.63% and 86.14%.
c. The proposed method generates a smooth feedrate profile, continuous acceleration curve and continuous jerk curve. Meanwhile, the actual maximum acceleration and jerk are under the confined range strictly.
d. Machining efficiency is greatly improved. Compared with two conventional method, the machining time have decreased by 7.27 to 75.11%.

To further improve machining quality and efficiency, future work will focus on analytical one-step corner for linear toolpath. In addition, to increase the generality of the local corner transition method, the toolpath composed of lines and arcs will also be considered.

Appendix 1. Proof process of Theorem 1

When trigonometric functions are used to express $\overrightarrow{n_1}$ and $\overrightarrow{n_2}$, $\overrightarrow{n_1} = l_1\overrightarrow{T_1} = l_1(cos\alpha, sin\alpha)^T = \left(u_0^2 - v_0^2, 2u_0v_0\right)^T/15$ and $\overrightarrow{n_2} = l_2\overrightarrow{T_2} = l_2(cos\beta, sin\beta)^T = \left(u_7^2 - v_7^2, 2u_7v_7\right)^T/15$. According to the half angle formula of trigonometric function, u_0, v_0, u_7 and v_7 can be written as $u_0 = \pm\sqrt{15l_1}cos\frac{\alpha}{2}$, $v_0 = \pm\sqrt{15l_1}sin\frac{\alpha}{2}$, $u_7 = \pm\sqrt{15l_2}cos\frac{\beta}{2}$ and $v_7 = \pm\sqrt{15l_2}sin\frac{\beta}{2}$, where u_0 and v_0, u_7 and v_7 take the same sign. Substituting the above four parameters into $\overrightarrow{m} = \frac{(u_0u_7 - v_0v_7, u_0v_7 + u_7v_0)^T}{15}$, $\overrightarrow{B_7B_8}$ can be written as $\overrightarrow{B_7B_8} = \overrightarrow{m} = \pm\sqrt{l_1l_2}\left(cos\frac{\alpha+\beta}{2}, sin\frac{\alpha+\beta}{2}\right)^T$. It is obvious that the length of $\overrightarrow{B_7B_8}$ equals to $\sqrt{l_1l_2}$. In addition, according to the sum-to-product trigonometric identities, $\overrightarrow{T_1} + \overrightarrow{T_2} = \left(2cos\frac{\alpha+\beta}{2}cos\frac{\alpha-\beta}{2}, 2sin\frac{\alpha+\beta}{2}cos\frac{\alpha-\beta}{2}\right)^T = 2cos\frac{\alpha-\beta}{2}\left(cos\frac{\alpha+\beta}{2}, sin\frac{\alpha+\beta}{2}\right)^T$. Since P_0P_1 and P_1P_2 are two different linear segments, and they are not on the same line, $cos\frac{\alpha-\beta}{2} \neq 0$ can be deduced. If $cos\frac{\alpha-\beta}{2} > 0$, $\frac{\overrightarrow{T_1}+\overrightarrow{T_2}}{\left|\overrightarrow{T_1}+\overrightarrow{T_2}\right|} = \left(cos\frac{\alpha+\beta}{2}, sin\frac{\alpha+\beta}{2}\right)^T$, let u_0 and v_0 take the same sign, then $\frac{\overrightarrow{B_7B_8}}{\left|\overrightarrow{B_7B_8}\right|} = \left(cos\frac{\alpha+\beta}{2}, sin\frac{\alpha+\beta}{2}\right)^T = \frac{\overrightarrow{T_1}+\overrightarrow{T_2}}{\left|\overrightarrow{T_1}+\overrightarrow{T_2}\right|}$. On the contrary, let u_0 and v_0 take different signs, then $\frac{\overrightarrow{B_7B_8}}{\left|\overrightarrow{B_7B_8}\right|} = -\left(cos\frac{\alpha+\beta}{2}, sin\frac{\alpha+\beta}{2}\right)^T = \frac{\overrightarrow{T_1}+\overrightarrow{T_2}}{\left|\overrightarrow{T_1}+\overrightarrow{T_2}\right|}$.

Appendix 2. Proof process of Theorem 2

According to Eq. (9), $\overrightarrow{B_4B_7} = \overrightarrow{B_4B_5} + \overrightarrow{B_5B_6} + \overrightarrow{B_6B_7} = \frac{398}{429}\overrightarrow{m} + \frac{889}{429}\overrightarrow{n_1}$. At the same time, $\overrightarrow{B_4B_7} = \overrightarrow{B_4Q_1} + \overrightarrow{Q_1B_7}$. Since $\overrightarrow{m}$ and $\overrightarrow{n_1}$ are two different vectors, $\overrightarrow{B_4B_7}$ has only unique expression when expressed by base $\{\overrightarrow{m}, \overrightarrow{n_1}\}$. Considering $\overrightarrow{B_4Q_1}$ and $\overrightarrow{n_1}$, $\overrightarrow{Q_1B_7}$ and $\overrightarrow{m}$ have the same directions, it can be deduced that $\overrightarrow{B_4Q_1} = \frac{889}{429}\overrightarrow{n_1}$ and $\overrightarrow{Q_1B_7} = \frac{398}{429}\overrightarrow{m}$, i.e. $\left|\overrightarrow{B_4Q_1}\right| = \frac{889}{429}l_1$. Similarly, $\left|\overrightarrow{B_{11}Q_2}\right| = \frac{889}{429}l_2$. From Theorem 1, it is known that B_7B_8 and the angle bisector of $\angle P_0P_1P_2$ are perpendicular. As shown in Fig. 1, the angle bisector of $\angle P_0P_1P_2$ and B_7B_8 intersect at point B_m; then, B_m is the midpoint of B_7B_8. In right triangle $\Delta Q_1P_1B_m$, $\left|\overrightarrow{B_mQ_1}\right| = \left|\overrightarrow{Q_1B_7}\right| + \frac{\left|\overrightarrow{B_7B_8}\right|}{2} = \frac{1225}{858}\sqrt{l_1l_2}$, $\angle Q_1P_1B_m = \frac{\pi-\theta}{2}$, then $\left|\overrightarrow{Q_1P_1}\right| = \frac{1225\sqrt{l_1l_2}}{858cos\frac{\theta}{2}}$. Similarly, $\left|\overrightarrow{Q_2P_1}\right| = \frac{1225\sqrt{l_1l_2}}{858cos\frac{\theta}{2}}$.

Appendix 3. Proof process of Theorem 3

When $l_1 = l_2$, the proposed PH spline is symmetrical about the angle bisector of $\angle P_0P_1P_2$; then, the maximum deviation error occurs between the mid-point of the proposed PH spline and corner point P_1, which can be expressed as

$$\begin{aligned} e_{max} = \left|r(0.5) - P_1\right| = \frac{1}{2^{15}}|&(B_0 - P_1) + 15(B_1 - P_1) \\ &+ 105(B_2 - P_1) + 455(B_3 - P_1) + 1365(B_4 - P_1) \\ &+ 3003(B_5 - P_1) + 5005(B_6 - P_1) + 6435(B_7 - P_1) \\ &+ 6435(B_8 - P_1) + 5005(B_9 - P_1) + 3003(B_{10} - P_1) \\ &+ 1365(B_{11} - P_1) + 455(B_{12} - P_1) + 105(B_{13} - P_1) \\ &+ 15(B_{14} - P_1) + (B_{15} - P_1)| = \frac{1}{2^{15}}|(B_0 + B_{15} - 2P_1) \\ &+ 15(B_1 + B_{14} - 2P_1) + 105(B_2 + B_{13} - 2P_1) \\ &+ 455(B_3 + B_{12} - 2P_1) + 1365(B_4 + B_{11} - 2P_1) \\ &+ 3003(B_5 + B_{10} - 2P_1) + 5005(B_6 + B_9 - 2P_1) \\ &+ 6435(B_7 + B_8 - 2P_1)|. \end{aligned} \tag{24}$$

From Eq. (10), it can be deduced that

$$\begin{cases} B_0 + B_{15} - 2P_1 = (4l_1 + \frac{889}{429}l_1 + l)(\overrightarrow{T_2} - \overrightarrow{T_1}) \\ B_1 + B_{14} - 2P_1 = (3l_1 + \frac{889}{429}l_1 + l)(\overrightarrow{T_2} - \overrightarrow{T_1}) \\ B_2 + B_{13} - 2P_1 = (2l_1 + \frac{889}{429}l_1 + l)(\overrightarrow{T_2} - \overrightarrow{T_1}) \\ B_3 + B_{12} - 2P_1 = (l_1 + \frac{889}{429}l_1 + l)(\overrightarrow{T_2} - \overrightarrow{T_1}) \\ B_4 + B_{11} - 2P_1 = (\frac{889}{429}l_1 + l)(\overrightarrow{T_2} - \overrightarrow{T_1}) \\ B_5 + B_{10} - 2P_1 = (\frac{490}{429}l_1 + l)(\overrightarrow{T_2} - \overrightarrow{T_1}) \\ B_6 + B_9 - 2P_1 = (\frac{175}{429}l_1 + l)(\overrightarrow{T_2} - \overrightarrow{T_1}) \\ B_7 + B_8 - 2P_1 = l(\overrightarrow{T_2} - \overrightarrow{T_1}) \end{cases}. \tag{25}$$

Combining Eqs. (24) and (25), the maximum deviation error $e_{\max}$ is expressed as

$$e_{\max} = \frac{1}{2^{15}}\left|\overrightarrow{T_2} - \overrightarrow{T_1}\right|\left(\left(\frac{397}{429} + 10207\right)l_1 + 16384l\right). \tag{26}$$

Considering $\left|\overrightarrow{T_2} - \overrightarrow{T_1}\right| = 2sin\left(\frac{\theta}{2}\right)$ and $l = \frac{16384\times1225}{858cos(\frac{\theta}{2})}\sqrt{l_1l_2} = \frac{16384\times1225}{858cos(\frac{\theta}{2})}l_1$, Eq. (13) can be obtained and Theorem 3 is proved.

Appendix 4. Proof process of Theorem 4

If $l_1 = l_2$, $R(t)$ is the same as $r(t)$ and $e_r = e_R$. Without loss of generality, translate, rotate and, if necessary, reflect transition PH spline such that P_1 is at the origin, P_0 is on the

negative x-axis, P_2 is above the x-axis and $l_1 > l_2$. Replace l_1 and l_2 in Eq. (10) with $l_0 = \max(l_1, l_2) = l_1$ to get the control points of $R(t)$, which is denoted by $\overline{B}_i (i = 0, 1, 2, \ldots, 15)$. Subtracting B_i from $\overline{B}_i$, we arrive at

$$
\begin{cases}
\overline{B}_0 - B_0 = -\frac{1225}{858cos\frac{\theta}{2}}\sqrt{l_1}(\sqrt{l_1} - \sqrt{l_2})\overrightarrow{T_1} \\
\overline{B}_1 - B_1 = -\frac{1225}{858cos\frac{\theta}{2}}\sqrt{l_1}(\sqrt{l_1} - \sqrt{l_2})\overrightarrow{T_1} \\
\overline{B}_2 - B_2 = -\frac{1225}{858cos\frac{\theta}{2}}\sqrt{l_1}(\sqrt{l_1} - \sqrt{l_2})\overrightarrow{T_1} \\
\overline{B}_3 - B_3 = -\frac{1225}{858cos\frac{\theta}{2}}\sqrt{l_1}(\sqrt{l_1} - \sqrt{l_2})\overrightarrow{T_1} \\
\overline{B}_4 - B_4 = -\frac{1225}{858cos\frac{\theta}{2}}\sqrt{l_1}(\sqrt{l_1} - \sqrt{l_2})\overrightarrow{T_1} \\
\overline{B}_5 - B_5 = -\frac{1195}{858cos\frac{\theta}{2}}\sqrt{l_1}\left(\sqrt{l_1} - \sqrt{l_2}\right)\overrightarrow{T_1} + \frac{10}{286cos\frac{\theta}{2}}\sqrt{l_1}\left(\sqrt{l_1} - \sqrt{l_2}\right)\overrightarrow{T_2} \\
\overline{B}_6 - B_6 = -\frac{1081}{858cos\frac{\theta}{2}}\sqrt{l_1}\left(\sqrt{l_1} - \sqrt{l_2}\right)\overrightarrow{T_1} + \frac{48}{286cos\frac{\theta}{2}}\sqrt{l_1}\left(\sqrt{l_1} - \sqrt{l_2}\right)\overrightarrow{T_2} \\
\overline{B}_7 - B_7 = -\frac{827}{858cos\frac{\theta}{2}}\sqrt{l_1}\left(\sqrt{l_1} - \sqrt{l_2}\right)\overrightarrow{T_1} + \frac{398}{858cos\frac{\theta}{2}}\sqrt{l_1}\left(\sqrt{l_1} - \sqrt{l_2}\right)\overrightarrow{T_2} \\
\overline{B}_8 - B_8 = -\frac{398}{858cos\frac{\theta}{2}}\sqrt{l_1}\left(\sqrt{l_1} - \sqrt{l_2}\right)\overrightarrow{T_1} + \frac{827}{286cos\frac{\theta}{2}}\sqrt{l_1}\left(\sqrt{l_1} - \sqrt{l_2}\right)\overrightarrow{T_2} \\
\overline{B}_9 - B_9 = -\frac{48}{286cos\frac{\theta}{2}}\sqrt{l_1}\left(\sqrt{l_1} - \sqrt{l_2}\right)\overrightarrow{T_1} + \left(\frac{175}{429}(l_1 - l_2) + \frac{1081}{858cos\frac{\theta}{2}}\sqrt{l_1}\left(\sqrt{l_1} - \sqrt{l_2}\right)\right)\overrightarrow{T_2} \\
\overline{B}_{10} - B_{10} = -\frac{10}{286cos\frac{\theta}{2}}\sqrt{l_1}\left(\sqrt{l_1} - \sqrt{l_2}\right)\overrightarrow{T_1} + \left(\frac{490}{429}(l_1 - l_2) + \frac{1195}{858cos\frac{\theta}{2}}\sqrt{l_1}\left(\sqrt{l_1} - \sqrt{l_2}\right)\right)\overrightarrow{T_2} \\
\overline{B}_{11} - B_{11} = \left(\frac{889}{429}(l_1 - l_2) + \frac{1225}{858cos\frac{\theta}{2}}\sqrt{l_1}\left(\sqrt{l_1} - \sqrt{l_2}\right)\right)\overrightarrow{T_2} \\
\overline{B}_{12} - B_{12} = \left(\left(\frac{889}{429} + 1\right)(l_1 - l_2) + \frac{1225}{858cos\frac{\theta}{2}}\sqrt{l_1}\left(\sqrt{l_1} - \sqrt{l_2}\right)\right)\overrightarrow{T_2} \\
\overline{B}_{13} - B_{13} = \left(\left(\frac{889}{429} + 2\right)(l_1 - l_2) + \frac{1225}{858cos\frac{\theta}{2}}\sqrt{l_1}\left(\sqrt{l_1} - \sqrt{l_2}\right)\right)\overrightarrow{T_2} \\
\overline{B}_{14} - B_{14} = \left(\left(\frac{889}{429} + 3\right)(l_1 - l_2) + \frac{1225}{858cos\frac{\theta}{2}}\sqrt{l_1}\left(\sqrt{l_1} - \sqrt{l_2}\right)\right)\overrightarrow{T_2} \\
\overline{B}_{15} - B_{15} = \left(\left(\frac{889}{429} + 4\right)(l_1 - l_2) + \frac{1225}{858cos\frac{\theta}{2}}\sqrt{l_1}\left(\sqrt{l_1} - \sqrt{l_2}\right)\right)\overrightarrow{T_2}
\end{cases}
\tag{27}
$$

It is obvious that $\overline{B}_i - B_i = a_i\overrightarrow{T_1} + b_i\overrightarrow{T_2}, a_i \le 0$ and $b_i \ge 0$ for $i = 0, 1, \ldots, 15$. Considering $r(t) = \sum_{i=0}^{15} B_i b_i^{15}(t)$ and $R(t) = \sum_{i=0}^{15} \overline{B}_i b_i^{15}(t)$, we have

$$
\overrightarrow{r(t)R(t)} = \sum_{i=0}^{15}\left(\overline{B}_i - B_i\right)b_i^{15}(t) = f_1(t)\overrightarrow{T_1} + f_2(t)\overrightarrow{T_2} \tag{28}
$$

where $f_1(t) \le 0$ and $f_2(t) \ge 0$ for arbitrary $t \in [0, 1]$. As shown in Fig. 24, the region bounded by the transition PH spline $r(t)$ and the linear trajectory P_0–$P_1 - P_2$ is denoted as S. Then, it can be deduced from Eq. (27) that $R(t)$ is outside of S for arbitrary $t \in [0, 1]$. From the convex hull property of Bezier spine, the transition PH spline $R(t)$ is inside of $\Delta P_0P_1P_2$. Then, for arbitrary $t_1 \in [0, 1]$, there is an intersection point between the line segment $\overline{P_1R(t_1)}$ and the transition PH spline $r(t)$; in other words, there is a $t_2 \in [0, 1]$ such that $\left|\overrightarrow{P_1r(t_2)}\right| \le \left|\overrightarrow{P_1R(t_1)}\right|$, which gives $e_r \le e_R$ naturally.

Appendix 5. Parameters of butterfly-shaped curve

The degree: $p = 3$.

The control point (mm): $P = [(54.493, 52.139), (55.507,52.139), (56.082, 49.615), (56.780, 44.971), (69.575,51.358), (77.786, 58.573), (90.526, 67.081), (105.973,63.801), (100.400, 47.326), (94.567, 39.913), (92.369,30.485), (83.440, 33.757), (91.892, 28.509), (89.444,20.393), (83.218, 15.446), (87.621, 4.830), (80.945, 9.267),(79.834, 14.535), (76.074, 8.522), (70.183, 12.550), (64.171,16.865), (59.993, 22.122), (55.680, 36.359), (56.925, 24.995),(59.765, 19.828), (54.493, 14.940), (49.220, 19.828), (52.060,24.994), (53.305, 36.359), (48.992, 22.122), (44.814, 16.865),(38.802, 12.551), (32.911, 8.521), (29.152, 14.535), (28.040,9.267), (21.364, 4.830), (25.768, 15.447), (19.539, 20.391),(17.097, 28.512), (25.537, 33.750), (16.602, 30.496), (14.199,39.803), (8.668, 47.408), (3.000, 63.794), (18.465, 67.084),(31.197, 58.572), (39.411, 51.358), (52.204, 44.971), (52.904,49.614), (53.478, 52.139), (54.492, 52.139)]$.

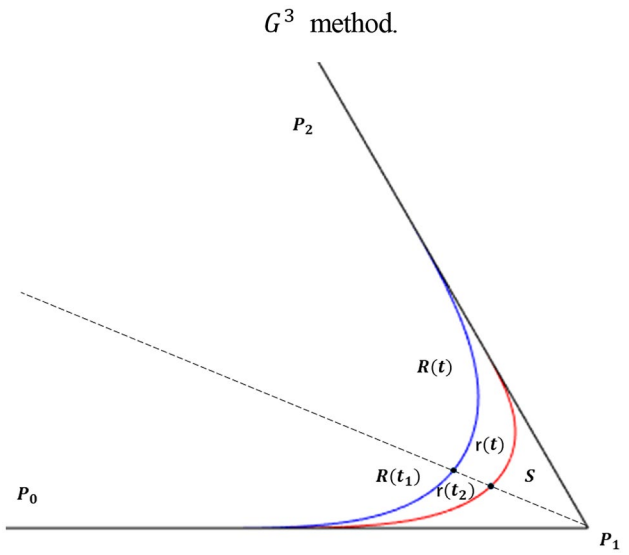

Fig. 24 The schematic diagram of two transition PH spline $r(t)$ and $R(t)$

The knot vector: $U = [0, 0, 0, 0, 0.0083, 0.015, 0.0361, 0.0855, 0.1293, 0.1509, 0.1931, 0.2273, 0.2435, 0.2561, 0.2692, 0.2889, 0.3170, 0.3316, 0.3482, 0.3553, 0.3649, 0.3837, 0.4005, 0.4269, 0.4510, 0.4660, 0.4891, 0.5000, 0.5109, 0.5340, 0.5489, 0.5731, 0.5994, 0.6163, 0.6351, 0.6447, 0.6518, 0.6683, 0.6830, 0.7111, 0.7307, 0.7439, 0.7565, 0.7729, 0.8069, 0.8491, 0.8707, 0.9145, 0.9639, 0.9850, 0.9917, 1.0, 1.0, 1.0, 1.0]$.

The weight vector: $W = [1.0, 1.0, 1.0, 1.2, 1.0, 1.0, 1.0, 1.0, 1.0, 1.0, 1, 2, 1.0, 1.0, 5.0, 3.0, 1.0, 1.1, 1.0, 1.0, 1.0, 1.0, 1.0, 1.0, 1.0, 1.0, 1.0, 1.0, 1.0, 1.0, 1.0, 1.0, 1.0, 1.1, 1.0, 3.0, 5.0, 1.0, 1.0, 2.0, 1.0, 1.0, 1.0, 1.0, 1.0, 1.0, 1.0, 1.2, 1.0, 1.0, 1.0]$.

Funding This work has been supported by the National Key Research and Development Program of China (Grant No.2020YFA0713700), the National Natural Science Foundation of China (Grants No. 12171023, No. 12001028 and No. 62102013) and funded by China Postdoctoral Science Foundation (Grant No. 2021M690303).

Availability of data and material Not applicable.

Code availability Not applicable.

Declarations

Ethics approval The research does not involve human participants and/or animals.

Consent to participate Consent to submit the paper for publication has been received explicitly from all co-authors.

Consent for publication All authors have read and agreed to publish the manuscript.

Conflict of interest The authors declare no competing interests.

References

1. Zhong W, Luo X, Chang W, Cai Y, Ding F, Liu H, Sun Y (2021) Toolpath interpolation and smoothing for computer numerical control machining of freeform surfaces: a review. Int J Autom Comput 17(1):1–16. https://doi.org/10.1007/s11633-019-1190-y
2. Wang W, Hu C, Zhou K, He S, Zhu L (2021) Local asymmetrical corner trajectory smoothing with bidirectional planning and adjusting algorithm for CNC machining. Robot Comput Integr Manuf 68:102058. https://doi.org/10.1016/j.rcim.2020.102058
3. Zhang Y, Zhao M, Ye P, Zhang H (2019) A G4 continuous b-spline transition algorithm for cnc machining with jerk-smooth feedrate scheduling along linear segments. Comput Aided Des 115:231–243. https://doi.org/10.1016/j.cad.2019.04.004
4. He S, Ou D, Yan C, Lee C (2015) A chord error conforming tool path B-spline fitting method for NC machining based on energy minimization and LSPIA. J Comput Des Eng 2(4):218–232. https://doi.org/10.1016/j.jcde.2015.06.002
5. Deng C, Lin H (2015) Progressive and iterative approximation for least squares B-spline curve and surface fitting. Comput Aided Des 47:32–44. https://doi.org/10.1016/j.cad.2013.08.012
6. Yang Z, Shen L, Yuan C, Gao X (2015) Curve fitting and optimal interpolation for CNC machining under confined error using quadratic B-splines. Comput Aided Des 66:62–72. https://doi.org/10.1016/j.cad.2015.04.010
7. Min K, Sun Y, Lee C, Hu P, He S (2019) An improved B-spline fitting method with arc-length parameterization, G2-continuous blending, and quality refinement. Int J Precis Eng Manuf 20(11):1939–1955. https://doi.org/10.1007/s12541-019-00210-0
8. Lin F, Shen L, Yuan C, Mi Z (2019) Certified space curve fitting and trajectory planning for CNC machining with cubic B-splines. Comput Aided Des 106:13–29. https://doi.org/10.1016/j.cad.2018.08.001
9. Hu Q, Chen Y, Jin X, Yang J (2019) A real-time C3 continuous local corner smoothing and interpolation algorithm for CNC machine tools. J Manuf Sci Eng 141(4):041004. https://doi.org/10.1115/1.4042606
10. Huang X, Zhao F, Tao T, Mei X (2021) A newly developed corner smoothing methodology based on clothoid splines for high speed machine tools. Robot Comput Integr Manuf 70:102106. https://doi.org/10.1016/j.rcim.2020.102106
11. Zhao H, Zhu L, Ding H (2013) A real-time look-ahead interpolation methodology with curvature-continuous B-spline transition scheme for CNC machining of short line segments. Int J Mach Tools Manuf 65:88–98. https://doi.org/10.1016/j.ijmachtools.2012.10.005
12. Sencer B, Shamoto E (2014) Curvature-continuous sharp corner smoothing scheme for Cartesian motion systems. IEEE 13th International Workshop on Advanced Motion Control, pp 374–379. https://doi.org/10.1109/AMC.2014.6823311
13. Du X, Huang J, Zhu L (2018) A locally optimal transition method with analytical calculation of transition length for computer numerical control machining of short line segments. Proc Inst Mech Eng B J Eng Manufe 232(13):2409–2419. https://doi.org/10.1177/0954405417697351
14. Jin Y, Bi Q, Wang Y (2015) Dual-Bezier path smoothing and interpolation for five-axis linear tool path in workpiece coordinate system. Adv Mech Eng 7(7):1–14. https://doi.org/10.1177/1687814015595211
15. Bi Q, Wang Y, Zhu L, Ding H (2011) A practical continuous-curvature Bézier transition algorithm for high-speed machining of linear tool path. Intelligent Robotics and Applications. https://doi.org/10.1007/978-3-642-25489-5_45

16. Tulsyan S, Altintas Y (2015) Local toolpath smoothing for five-axis machine tools. Int J Mach Tools Manuf 96:15–26. https://doi.org/10.1016/j.ijmachtools.2015.04.014
17. Fan W, Lee C, Chen J (2015) A realtime curvature-smooth interpolation scheme and motion planning for CNC machining of short line segments. Int J Mach Tools Manuf 96:27–46. https://doi.org/10.1016/j.ijmachtools.2015.04.009
18. Zhang Y, Wang T, Dong J, Peng P, Liu Y, Ke R (2020) An analytical G3 continuous corner smoothing method with adaptive constraints adjustments for five-axis machine tool. Int J Adv Manuf Technol 109:1007–1026. https://doi.org/10.1007/s00170-020-05402-x
19. Xie Z, Xie F, Liu X, Wang J (2021) Global G3 continuity toolpath smoothing for a 5-DoF machining robot with parallel kinematics. Robot Comput Integr Manuf 67:102018. https://doi.org/10.1016/j.rcim.2020.102018
20. Petrinić T, Brezak M, Petrović I (2017) Time-optimal velocity planning along predefined path for static formations of mobile robots. Int J Control Autom Syst 15(1):293–302. https://doi.org/10.1007/s12555-015-0192-y
21. Frego M, Bertolazzi E, Biral F, Fontanelli D, Palopoli L (2017) Semi-analytical minimum time solutions with velocity constraints for trajectory following of vehicles. Automatica 86:18–28. https://doi.org/10.1016/j.automatica.2017.08.020
22. Shahzadeh A, Khosravi A, Robinette T, Nahavandi S (2018) Smooth path planning using biclothoid fillets for high speed CNC machines. Int J Mach Tools Manuf 132:36–49. https://doi.org/10.1016/j.ijmachtools.2018.04.003
23. Xiao Q, Wan M, Liu Y, Qin X, Zhang W (2020) Space corner smoothing of CNC machine tools through developing 3D general clothoid. Robot Comput Integr Manuf 64:101949. https://doi.org/10.1016/j.rcim.2020.101949
24. Huang X, Zhao F, Tao T, Mei X (2020) A novel local smoothing method for five-axis machining with time-synchronization feedrate scheduling. IEEE Access 8:89185–89204. https://doi.org/10.1109/ACCESS.2020.2992022
25. Walton D, Meek D (2009) G2 blends of linear segments with cubics and Pythagorean-hodograph quintics. Int J Comput Math 86(9):1498–1511. https://doi.org/10.1080/00207160701828157
26. Imani B, Ghandehariun A (2011) Real-time PH-based interpolation algorithm for high speed CNC machining. Int J Adv Manuf Technol 56:619–629. https://doi.org/10.1007/s00170-011-3200-2
27. Farouki R (2014) Construction of G2 rounded corners with Pythagorean-hodograph curves. Comput Aided Geom Des 31:127–139. https://doi.org/10.1016/j.cagd.2014.02.002
28. Shi J, Bi Q, Wang Y, Liu G (2014) Development of real-time look-ahead methodology based on quintic ph curve with G2 continuity for high-speed machining. Appl Mech Mater 464:258–264. https://doi.org/10.4028/www.scientific.net/AMM.464.258
29. Shi J, Bi Q, Zhu L, Wang Y (2015) Corner rounding of linear five-axis tool path by dual PH curves blending. Int J Mach Tools Manuf 88:223–236. https://doi.org/10.1016/j.ijmachtools.2014.09.007
30. Wan M, Qin X, Xiao Q, Liu Y, Zhang W (2021) Asymmetrical pythagorean-hodograph (PH) spline-based C3 continuous corner smoothing algorithm for five-axis tool paths with short segments. J Manuf Process 64(3):1387–1411. https://doi.org/10.1016/j.jmapro.2021.02.059
31. Lee A, Lin M, Pan Y, Lin W (2011) The feedrate scheduling of NURBS interpolator for CNC machine tools. Comput Aided Des 43(6):612–628. https://doi.org/10.1016/j.cad.2011.02.014
32. Hu Y, Jiang X, Huo G, Su C, Wang B, Li H, Zheng Z (2021) A novel S-shape based NURBS interpolation with acc-jerk - continuity and round-off error elimination. arXiv:2103.14433
33. Su C, Jiang X, Huo G, Sun Y, Zheng Z (2020) Initial tool path selection of the iso-scallop method based on offset similarity analysis for global preferred feed directions matching. Int J Adv Manuf Technol 106:2675–2687. https://doi.org/10.1007/s00170-019-04789-6